

Supporting Information

Modulation of the intramolecular hydrogen bonding and push-pull electron effects toward realizing highly efficient organic room temperature phosphorescence

Guoyu Jiang,^{a†} Qiyao Li,^{b†} Anqi Lv,^{c†} Lingxiu Liu,^a Jianye Gong,^a Huili Ma,^{*c} Jianguo Wang,^{*a} and Ben Zhong Tang^{*b}

^a College of Chemistry and Chemical Engineering, Inner Mongolia Key Laboratory of Fine Organic Synthesis, Inner Mongolia University, Hohhot 010021, P.R. China. Email: wangjg@iccas.ac.cn.

^b School of Science and Engineering, Shenzhen Key Laboratory of Functional Aggregate Materials, The Chinese University of Hong Kong, Shenzhen, Guangdong 518172, P.R. China. Email: tangbenz@cuhk.edu.cn.

^c Key Laboratory of Flexible Electronics (KLOFE) & Institute of Advanced Materials (IAM), Nanjing Tech University (NanjingTech), 30 South Puzhu Road, Nanjing 211816, P.R. China. Email: iamhlma@njtech.edu.cn.

† These authors contributed equally to this work.

Table of Contents

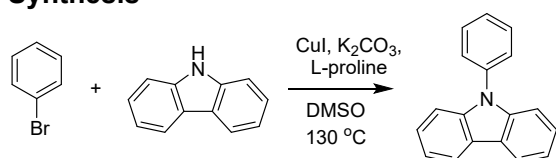
Experimental Procedures	S3-S5
Materials and instrumentation	S3
Synthesis	S3-S5
Density functional theory calculations	S5
Figures and tables	S6-S32
References	S33

Experimental Procedures

Materials and instrumentation.

All Chemicals were purchased from Tansoole, Innochem, J&K chemistry, Sigma-Aldrich and TCI, and used directly without further purification. ^1H NMR and ^{13}C NMR spectra were recorded with a Bruker ARX 400 MHz or Avance II 500 MHz NMR spectrometer. High resolution mass spectra (HRMS) were recorded on a GCT premier CAB048 mass spectrometer operating in a MALDI-TOF mode. Steady-state and transient photoluminescence (PL) spectra were recorded on Horiba FL3 Spectrofluorometer. Time-resolved emission spectra were recorded on a Horiba DeltaFlex lifetime fluorescence spectrofluorometer. The absolute fluorescence quantum yield was measured using a Hamamatsu quantum yield spectrometer C11347 Quantaaurus QY. Single crystal X-ray diffraction was performed on a D/max-2550 PC X-ray diffractometer (XRD; Rigaku, Cu-K α radiation). The crystal data were collected on an Oxford Diffraction Xcalibur Atlas Gemini ultra instrument. High performance liquid chromatography (HPLC) was performed on an Agilent 1260 Infinite HPLC system using an Agilent 5 Prep-C18 column. The running rate was 10 mL/min, and the eluent were 80% acetonitrile and 20% water.

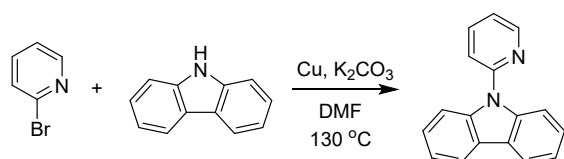
Synthesis



Scheme S1. Synthetic route to compound CzPh.

Synthesis of compound CzPh:

Into a 100 mL round-bottom flask, carbazole (1.0 g, 6.0 mmol) was dissolved in dry DMSO (20 mL). Then, bromobenzene (1.4 g, 9.0 mmol), K₂CO₃ (1.7 g, 12.0 mmol), L-proline (0.07 g, 0.6 mmol) and CuI (0.11 g, 0.6 mmol) were added. The reaction mixture was heated at 130 °C for 24 hours, and monitored by the thin layer chromatography (TLC). When the starting material was consumed completely, the reaction was cooled down to room temperature. The reaction mixture was extracted with water (80 mL) and ethyl acetate (3 × 70 mL). The combined organic layer was washed with brine solution (3 × 100 mL), dried over anhydrous Na₂SO₄, filtered and the solvent was evaporated via rotary evaporator. The crude product was purified by silica-gel column chromatography using hexane as the eluent. The white color solid was further recrystallized three times by using methanol, petroleum ether/ethyl acetate and petroleum ether/dichloromethane as the solvent respectively to afford the pure product (1.2 g, 85%). ^1H NMR (400 MHz, DMSO-*d*₆) δ (ppm): 8.24 (d, *J* = 7.6 Hz, 2H), 7.70 – 7.64 (m, 2H), 7.63 – 7.58 (m, 2H), 7.53 (t, *J* = 7.3 Hz, 1H), 7.42 (td, *J* = 7.5, 1.2 Hz, 2H), 7.36 (dt, *J* = 8.2, 1.0 Hz, 2H), 7.28 (ddd, *J* = 7.9, 6.9, 1.2 Hz, 2H). ^{13}C NMR (125 MHz, CDCl₃) δ (ppm): 140.90, 137.72, 129.86, 127.45, 127.16, 125.91, 123.34, 120.29, 119.88, 109.76. HRMS (MALDI-TOF): *m/z*: [M+H]⁺ calcd for C₁₈H₁₄N: 244.11262; found: 244.11208.

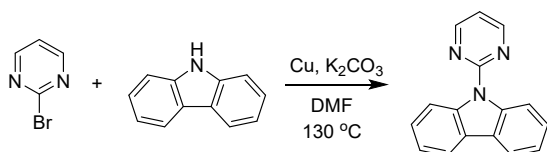


Scheme S2. Synthetic route to compound CzPy.

Synthesis of compound CzPy:

Into a 100 mL round-bottom flask, carbazole (1.0 g, 6.0 mmol) was dissolved in dry DMF (20 mL). Then, 2-bromopyridine (1.4 g, 9.0 mmol), K₂CO₃ (1.7 g, 12.0 mmol), and Cu powder (0.19 g, 3.0 mmol) were added. The reaction mixture was heated at 130 °C for 24 hours. After cooling down to room temperature, the solvent DMF was partly removed under reduced pressure. The residual mixture was extracted with water (80 mL) and ethyl acetate (3 × 70 mL). The combined organic layer was washed with brine solution (3 × 100 mL), dried over anhydrous Na₂SO₄, filtered and the solvent was evaporated via rotary evaporator. The crude product was purified by silica-gel column chromatography using hexane/ethyl acetate as the eluent. The white color solid was further recrystallized three times by using methanol, petroleum ether/ethyl acetate and petroleum ether/dichloromethane as the solvent respectively to afford the pure product (1.3 g, 87%). ^1H NMR (400 MHz, DMSO-*d*₆) δ (ppm): 8.74

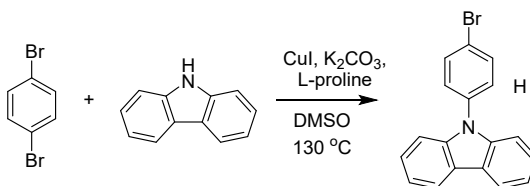
(ddd, $J = 4.9, 2.0, 0.9$ Hz, 1H), 8.24 (d, $J = 7.5$ Hz, 2H), 8.10 (ddd, $J = 8.1, 7.4, 2.0$ Hz, 1H), 7.81 (dt, $J = 8.3, 0.9$ Hz, 2H), 7.77 (dt, $J = 8.1, 1.0$ Hz, 1H), 7.50 – 7.43 (m, 3H), 7.33 (ddd, $J = 8.0, 7.2, 1.0$ Hz, 2H). ^{13}C NMR (125 MHz, CDCl_3) δ (ppm): 151.84, 149.66, 139.59, 138.48, 126.26, 124.33, 121.25, 120.95, 120.25, 119.08, 111.177. HRMS (MALDI-TOF): m/z : $[\text{M}+\text{H}]^+$ calcd for $\text{C}_{17}\text{H}_{13}\text{N}_2$: 245.10787; found: 245.10732.



Scheme S3. Synthetic route to compound CzPM.

Synthesis of compound CzPM:

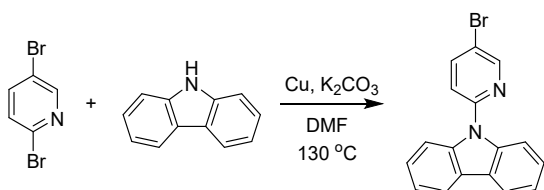
Into a 100 mL round-bottom flask, carbazole (1.0 g, 6.0 mmol) was dissolved in dry DMF (20 mL). Then, 2-bromopyrimidine (1.4 g, 9.0 mmol), K_2CO_3 (1.7 g, 12.0 mmol), and Cu powder (0.19 g, 3.0 mmol) were added. The reaction mixture was heated at 130 °C for 24 hours. After cooling down to room temperature, the solvent DMF was partly removed under reduced pressure. The residual mixture was extracted with water (80 mL) and ethyl acetate (3×70 mL). The combined organic layer was washed with brine solution (3×100 mL), dried over anhydrous Na_2SO_4 , filtered and the solvent was evaporated via rotary evaporator. The crude product was purified by silica-gel column chromatography using hexane/ethyl acetate as the eluent. The white color solid was further recrystallized three times by using methanol, petroleum ether/ethyl acetate and petroleum ether/dichloromethane as the solvent respectively to afford the pure product (1.4 g, 94%). ^1H NMR (400 MHz, $\text{DMSO}-d_6$) δ (ppm): 9.00 (d, $J = 4.8$ Hz, 2H), 8.81 (d, $J = 8.5$ Hz, 2H), 8.23 (ddd, $J = 7.8, 1.4, 0.7$ Hz, 2H), 7.53 (ddd, $J = 8.5, 7.2, 1.4$ Hz, 2H), 7.42 (t, $J = 4.8$ Hz, 1H), 7.39 (ddd, $J = 7.7, 7.4, 1.0$ Hz, 2H). ^{13}C NMR (125 MHz, CDCl_3) δ (ppm): 159.19, 157.87, 139.17, 126.60, 125.80, 122.28, 119.52, 116.24, 115.97. HRMS (MALDI-TOF): m/z : $[\text{M}+\text{H}]^+$ calcd for $\text{C}_{16}\text{H}_{12}\text{N}_3$: 246.10312; found: 246.10257.



Scheme S4. Synthetic route to compound CzPhBr.

Synthesis of compound CzPhBr:

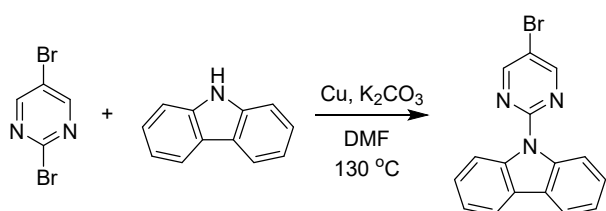
Into a 100 mL round-bottom flask, carbazole (1.0 g, 6.0 mmol) was dissolved in dry DMSO (20 mL). Then, 1,4-dibromobenzene (2.1 g, 9.0 mmol), K_2CO_3 (1.7 g, 12.0 mmol), L-proline (0.07 g, 0.6 mmol) and CuI (0.11 g, 0.6 mmol) were added. The reaction mixture was heated at 130 °C for 24 hours. After cooling down to room temperature, the reaction mixture was extracted with water (80 mL) and ethyl acetate (3×70 mL). The combined organic layer was washed with brine solution (3×100 mL), dried over anhydrous Na_2SO_4 , filtered and the solvent was evaporated via rotary evaporator. The crude product was purified by silica-gel column chromatography using hexane as the eluent. The white color solid was further recrystallized three times by using methanol, petroleum ether/ethyl acetate and petroleum ether/dichloromethane as the solvent respectively to afford the pure product (1.4 g, 72%). ^1H NMR (400 MHz, $\text{DMSO}-d_6$) δ (ppm): 8.25 (d, $J = 7.7$ Hz, 2H), 7.86 (d, $J = 7.7$ Hz, 2H), 7.60 (d, $J = 7.9$ Hz, 2H), 7.44 (t, $J = 8.2$ Hz, 2H), 7.40 (t, $J = 8.0$ Hz, 2H), 7.30 (t, $J = 7.3$ Hz, 2H). ^{13}C NMR (125 MHz, CDCl_3) δ (ppm): 140.63, 136.82, 133.12, 128.73, 126.09, 123.50, 120.90, 120.40, 120.22, 109.55. HRMS (MALDI-TOF): m/z : $[\text{M}+\text{H}]^+$ calcd for $\text{C}_{18}\text{H}_{13}\text{BrN}$: 322.02314; found: 322.02259.



Scheme S5. Synthetic route to compound CzPyBr.

Synthesis of compound CzPyBr:

Into a 100 mL round-bottom flask, carbazole (1.0 g, 6.0 mmol) was dissolved in dry DMF (20 mL). Then, 2,5-dibromopyridine (2.1 g, 9.0 mmol), K_2CO_3 (1.7 g, 12.0 mmol), and Cu powder (0.19 g, 3.0 mmol) were added. The reaction mixture was heated at 130 °C for 24 hours. After cooling down to room temperature, the solvent DMF was partly removed under reduced pressure. The residual mixture was extracted with water (80 mL) and ethyl acetate (3 × 70 mL). The combined organic layer was washed with brine solution (3 × 100 mL), dried over anhydrous Na_2SO_4 , filtered and the solvent was evaporated via rotary evaporator. The crude product was purified by silica-gel column chromatography using hexane/ethyl acetate as the eluent. The white color solid was further recrystallized three times by using methanol, petroleum ether/ethyl acetate and petroleum ether/dichloromethane as the solvent respectively to afford the pure product (1.4 g, 70%). 1H NMR (500 MHz, Chloroform-*d*) δ (ppm): 8.80 (d, J = 2.5 Hz, 1H), 8.14 (d, J = 7.8 Hz, 2H), 8.06 (dd, J = 8.5, 2.5 Hz, 1H), 7.85 (d, J = 8.2 Hz, 2H), 7.60 (d, J = 8.6 Hz, 1H), 7.48 (ddd, J = 8.4, 7.2, 1.3 Hz, 2H), 7.36 (t, J = 7.5 Hz, 2H). ^{13}C NMR (125 MHz, $CDCl_3$) δ (ppm): 150.55, 150.47, 141.01, 139.27, 126.40, 124.49, 121.32, 120.32, 119.95, 116.90, 111.13. HRMS (MALDI-TOF): m/z : $[M+H]^+$ calcd for $C_{17}H_{12}BrN_2$: 323.01839; found: 323.01784.



Scheme S6. Synthetic route to compound CzPMBR.

Synthesis of compound CzPMBR:

Into a 100 mL round-bottom flask, carbazole (1.0 g, 6.0 mmol) was dissolved in dry DMF (20 mL). Then, 2,5-dibromopyrimidine (2.1 g, 9.0 mmol), K_2CO_3 (1.7 g, 12.0 mmol), and Cu powder (0.19 g, 3.0 mmol) were added. The reaction mixture was heated at 130 °C for 24 hours. After cooling down to room temperature, the solvent DMF was partly removed under reduced pressure. The residual mixture was extracted with water (80 mL) and ethyl acetate (3 × 70 mL). The combined organic layer was washed with brine solution (3 × 100 mL), dried over anhydrous Na_2SO_4 , filtered and the solvent was evaporated via rotary evaporator. The crude product was purified by silica-gel column chromatography using hexane/ethyl acetate as the eluent. The white color solid was further recrystallized three times by using methanol, petroleum ether/ethyl acetate and petroleum ether/dichloromethane as the solvent respectively to afford the pure product (1.2 g, 60%). 1H NMR (400 MHz, DMSO-*d*₆) δ (ppm): 9.14 (s, 2H), 8.75 (dt, J = 8.4, 0.9 Hz, 2H), 8.25 (dq, J = 7.8, 0.7 Hz, 2H), 7.54 (ddd, J = 8.5, 7.2, 1.4 Hz, 2H), 7.42 (td, J = 7.5, 1.0 Hz, 2H). ^{13}C NMR (125 MHz, $CDCl_3$) δ (ppm): 158.21, 157.26, 138.91, 126.75, 125.97, 122.67, 119.58, 116.40, 112.87. HRMS (MALDI-TOF): m/z : $[M+H]^+$ calcd for $C_{16}H_{11}BrN_3$: 324.01363; found: 324.01309.

Density functional theory calculations

All equilibrium geometries in ground (S_0) and the lowest triplet (T_1) states were optimized based on QM/MM model (a 5x5x5 supercell) theory with two-layer ONIOM method from the crystal structure at B3LYP/def2-SVP level, therein the T_1 geometries were obtained using unrestricted density functional theory (DFT), taking CzPMBR as example shown in Figure S62. The central and surrounding molecule as active QM and rigid MM parts in QM/MM calculations to simulate crystalline environment, respectively. We further evaluated the excited state electronic structures based on T_1 geometries at B3LYP/def2-SVP level, including excitation energies, natural transition orbitals (NTOs) and spin-orbit couplings (SOCs) matrix elements between singlet and triplet states. The SOC matrix elements were performed by Beijing Density Function (BDF) program [1-2]. Other results were evaluated using Gaussian 09 package [3].

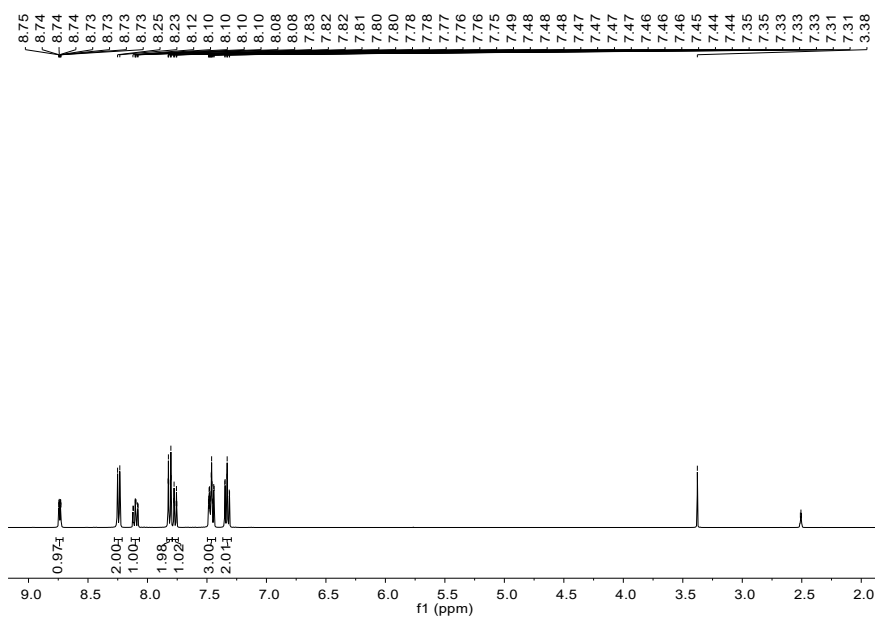


Figure S4. ^1H NMR spectrum of CzPy in d_6 -DMSO.

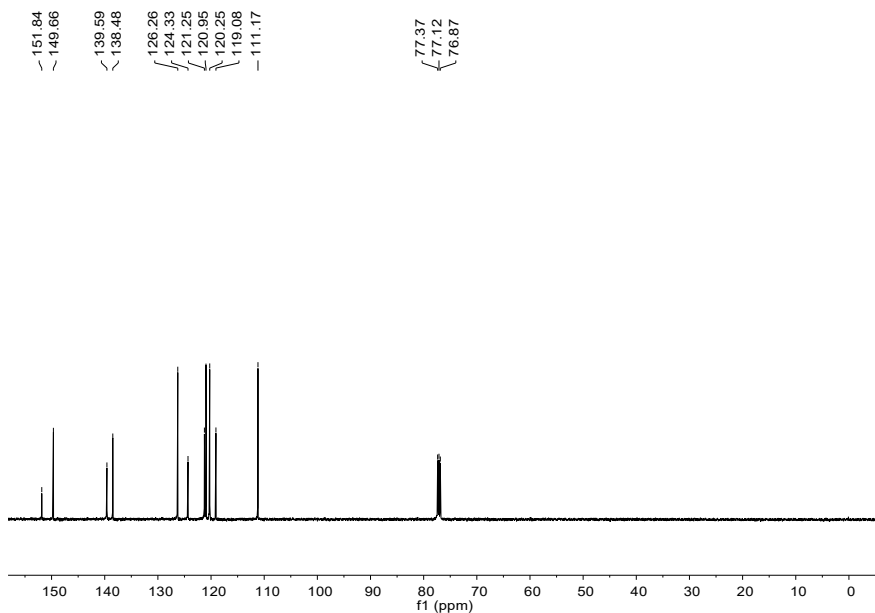


Figure S5. ^{13}C NMR spectrum of CzPy in CDCl_3 .

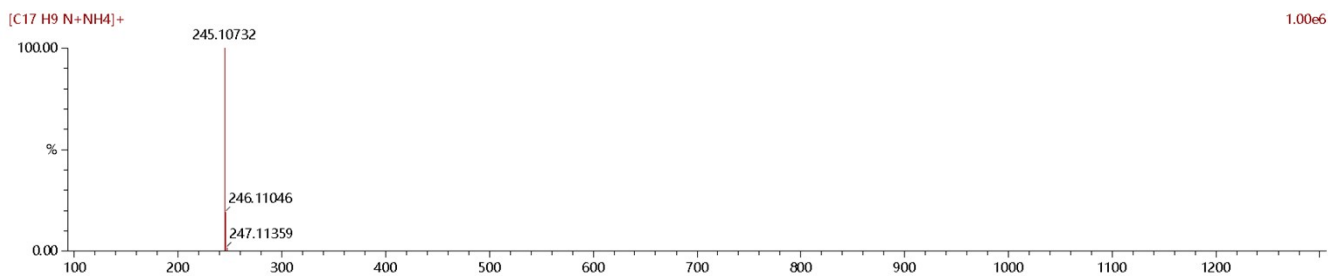


Figure S6. HRMS spectrum of CzPy.

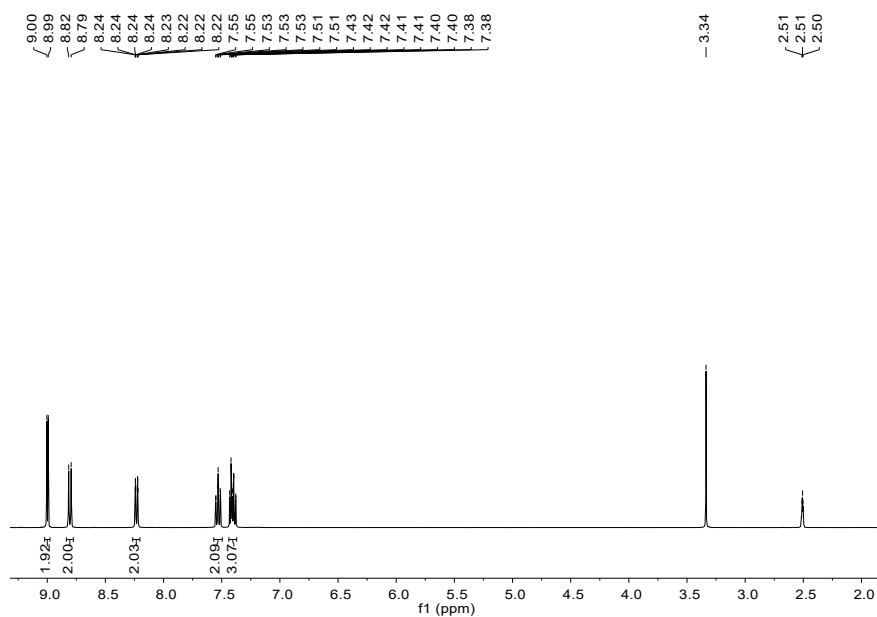


Figure S7. ^1H NMR spectrum of CzPM in d_6 -DMSO.

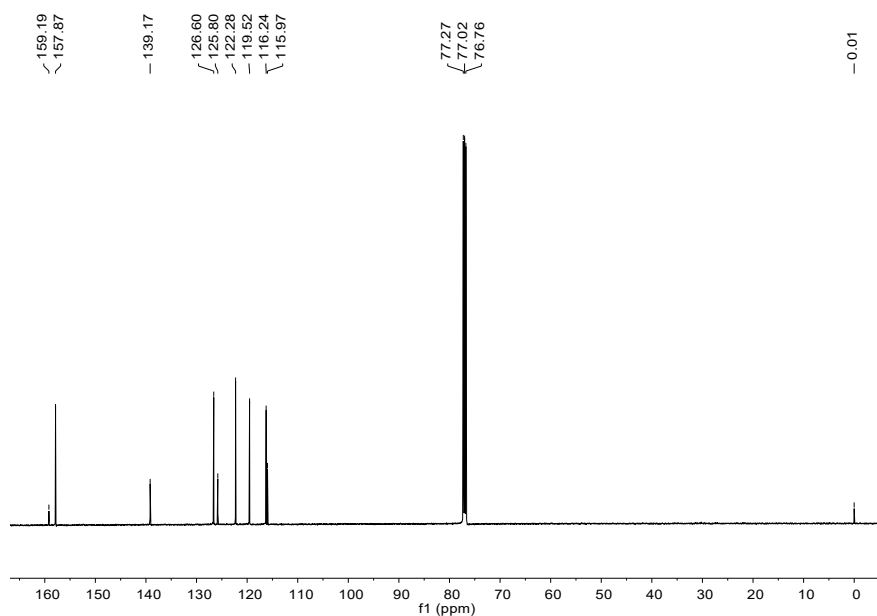


Figure S8. ^{13}C NMR spectrum of CzPM in CDCl_3 .

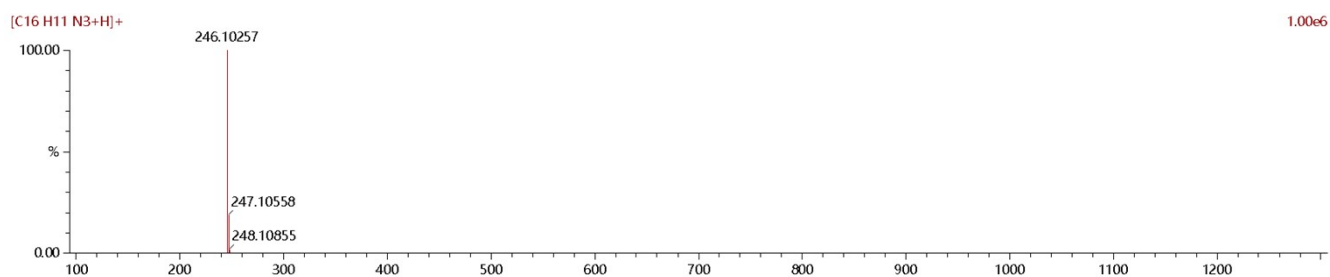


Figure S9. HRMS spectrum of CzPM.

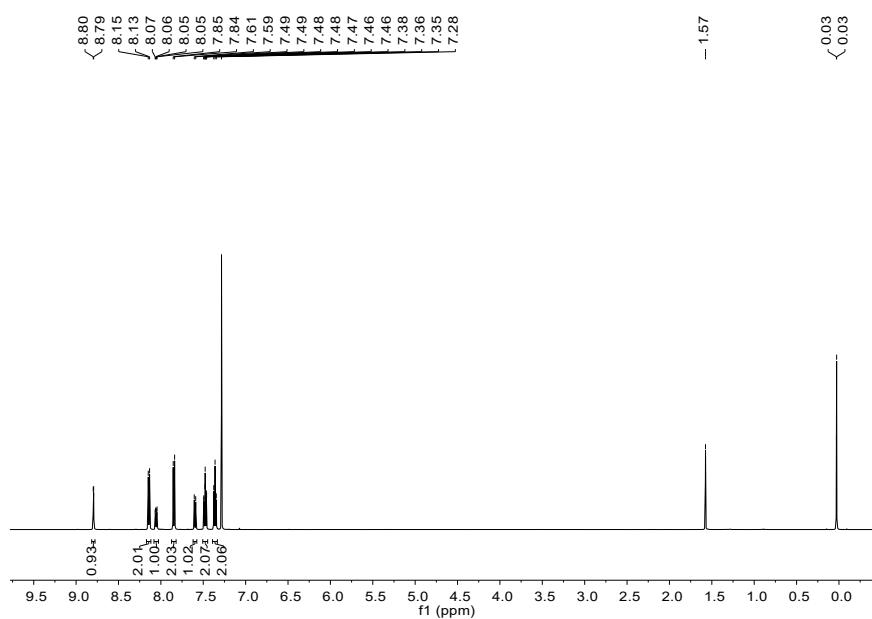


Figure S13. ^1H NMR spectrum of CzPyBr in CDCl_3 .

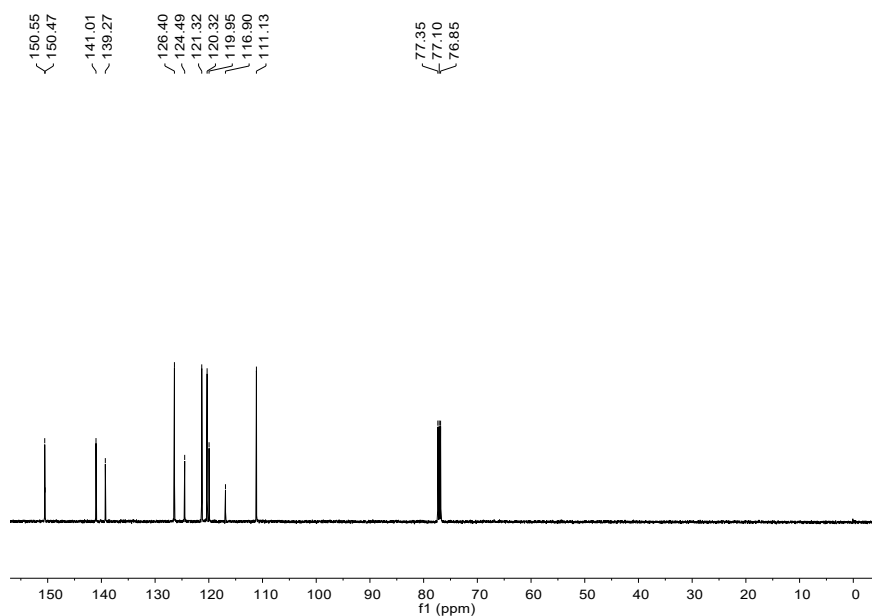


Figure S14. ^{13}C NMR spectrum of CzPyBr in CDCl_3 .

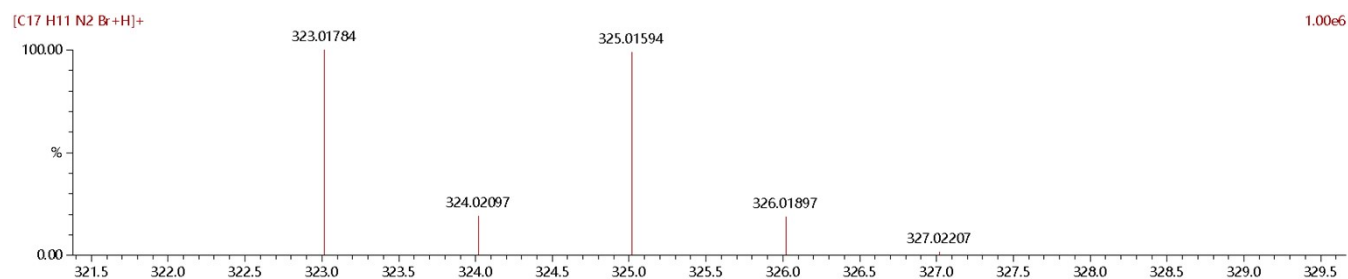


Figure S15. HRMS spectrum of CzPyBr.

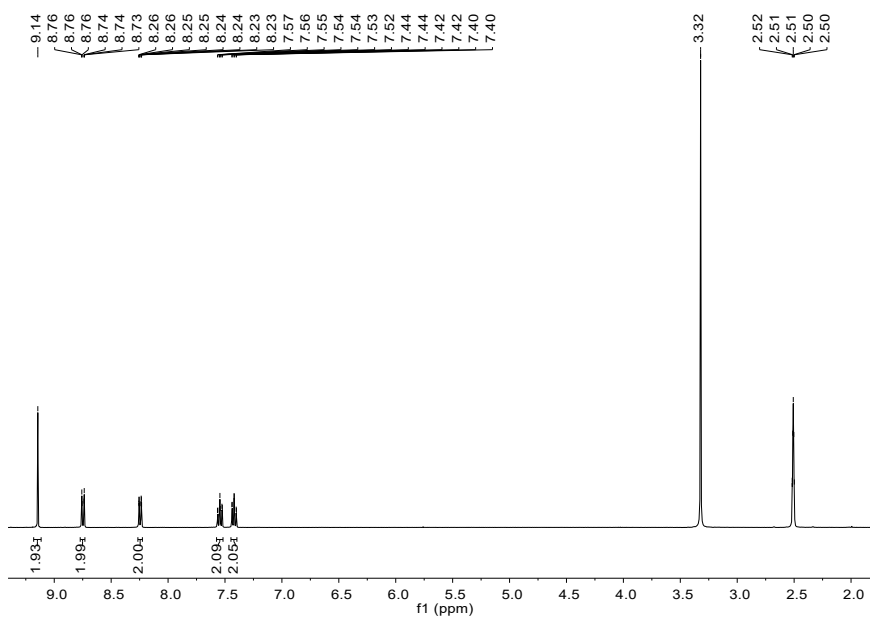


Figure S16. ^1H NMR spectrum of CzPMBr in d_6 -DMSO.

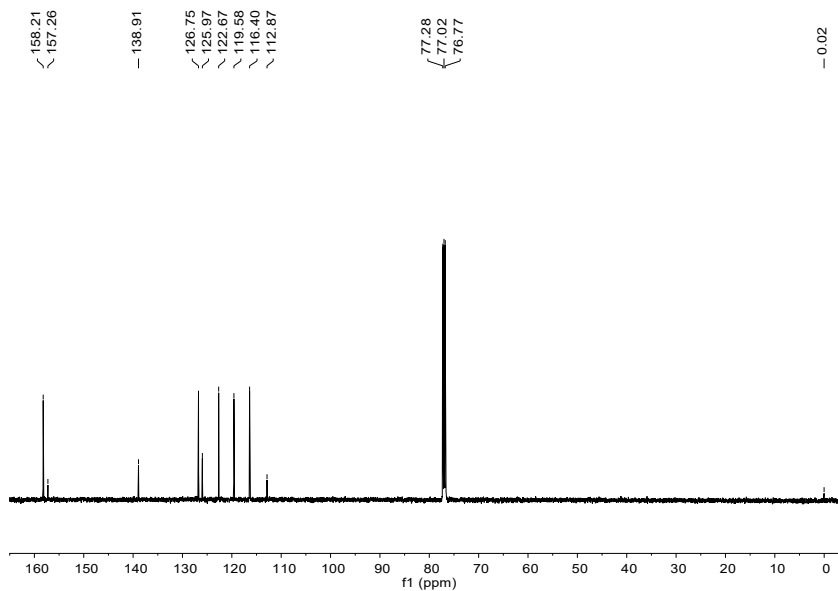


Figure S17. ^{13}C NMR spectrum of CzPMBr in CDCl_3 .

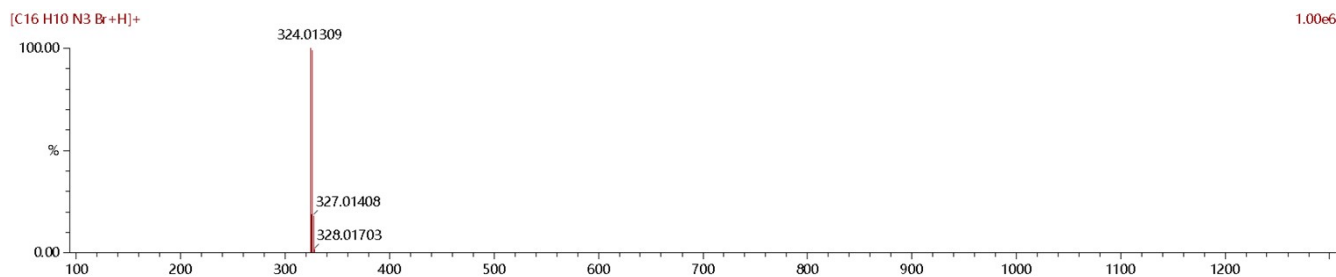


Figure S18. HRMS spectrum of CzPMBr.

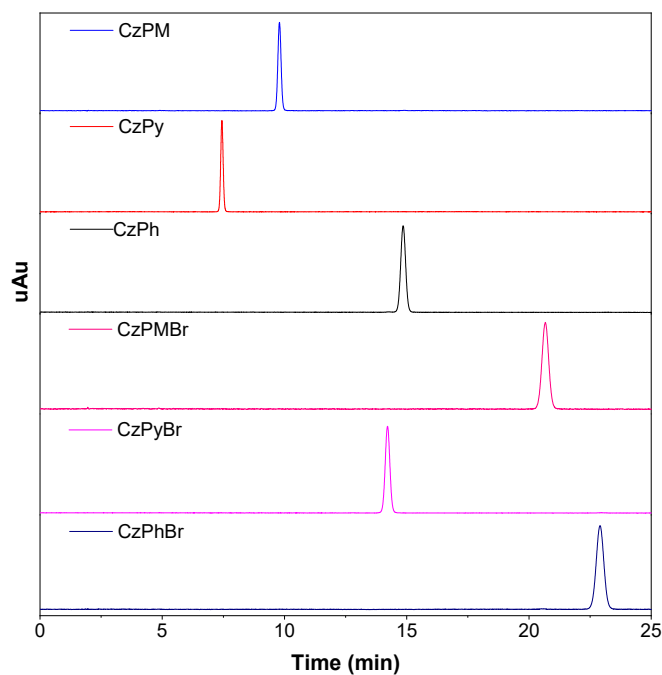


Figure S19. HPLC spectrum of CzPh, CzPy, CzPM, CzPhBr, CzPyBr and CzPMBR.

Table S1. Crystallographic and structural refinement data of CzPh, CzPy, CzPM, CzPhBr, CzPyBr and CzPMBR.^[a]

Identification code	CzPh	CzPy	CzPM	CzPhBr	CzPyBr	CzPMBR
Empirical formula	C ₁₈ H ₁₃ N	C ₁₇ H ₁₂ N ₂	C ₁₆ H ₁₁ N ₃	C ₁₈ H ₁₂ BrN	C ₁₇ H ₁₁ BrN ₂	C ₁₆ H ₁₀ BrN ₃
Formula weight	243.29	244.29	245.28	322.20	323.19	324.18
Temperature (K)	99.99(10)	99.97(10)	99.94(15)	100.02(10)	100.00(10)	296(2)
Crystal system	monoclinic	monoclinic	monoclinic	monoclinic	monoclinic	orthorhombic
space group	P 1 21/c1	P 1 21/n1	C 1 2/c1	P 1 21/c1	P 1 21/c1	P c a 21
a (Å)	14.2558(8)	14.3832(2)	25.4249(16)	8.42117(15)	11.6198(2)	17.8257(12)
b (Å)	10.8126(4)	11.72436(15)	5.1479(3)	20.1472(4)	7.12537(14)	13.1338(8)
c (Å)	17.9094(10)	16.3283(3)	19.2278(14)	8.63599(18)	16.4875(3)	5.5743(3)
α (deg)	90	90	90	90	90	90
β (deg)	112.874(7)	114.6388(18)	111.349(8)	108.529(2)	102.047(2)	90
γ (deg)	90	90	90	90	90	90
Volume (Å ³)	2543.5(2)	2502.81(7)	2343.9(3)	1389.26(5)	1335.03(5)	1305.05(14)
Z	8	8	8	4	4	4

^[a] Crystallographic data for the structures reported in this paper have been deposited with the Cambridge Crystallographic Data Centre as supplementary. Publication no. CCDC: 2085870 for CzPh, 2085871 for CzPy, 2085872 for CzPM, 2085873 for CzPhBr, 2085874 for CzPyBr and 2085875 for CzPMBR.

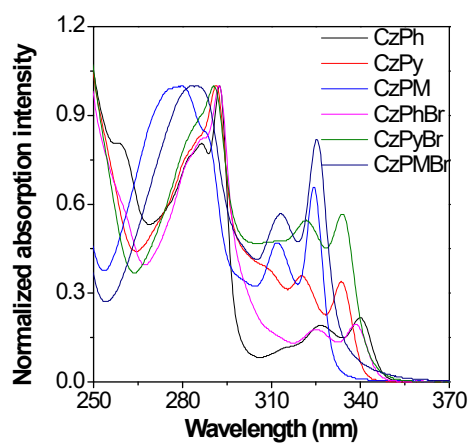


Figure S20. Absorption spectra of CzPh, CzPy, CzPM, CzPhBr, CzPyBr, CzPMBr in THF. Concentration=10 μ M.

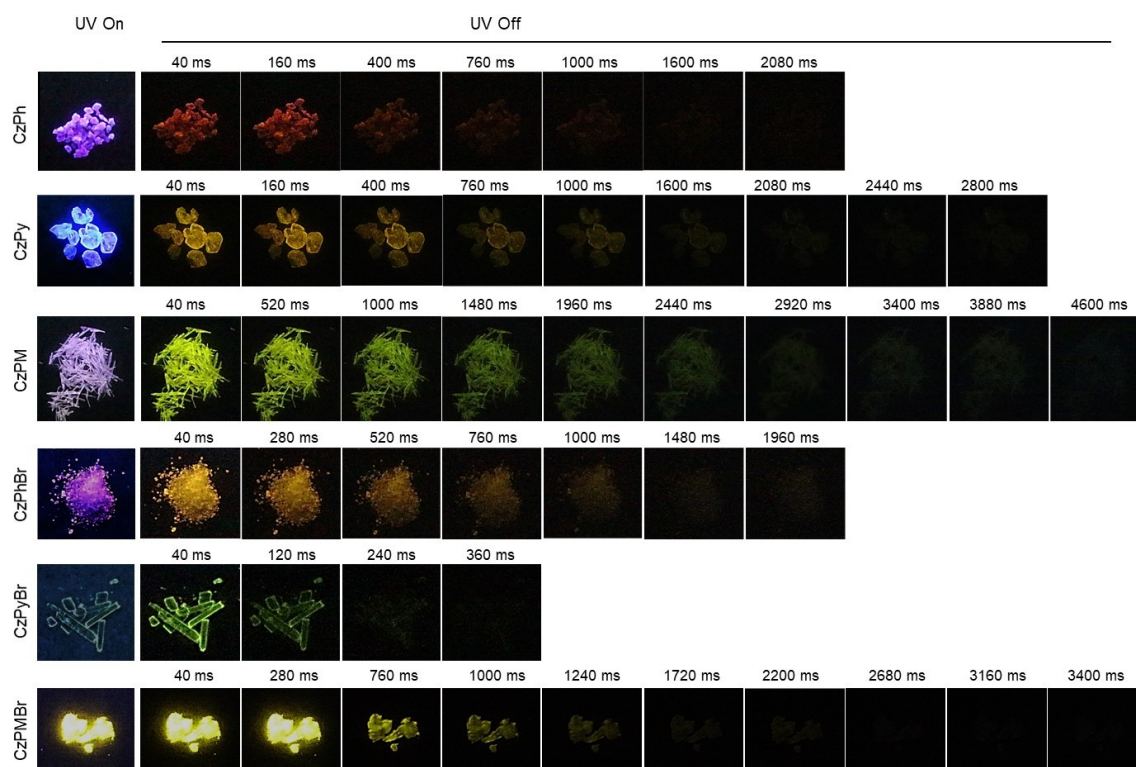


Figure S21. Photographs of CzPh, CzPy, CzPM, CzPhBr, CzPyBr, CzPMBr taken at different times, before and after turning off the 365 nm UV irradiation under ambient conditions.

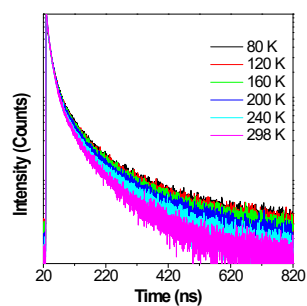


Figure S22. Time-resolved decay of the fluorescence (@430 nm) of CzPh in the crystalline state at different temperature.

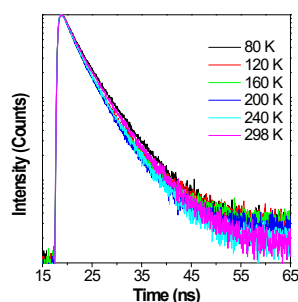


Figure S23. Time-resolved decay of the fluorescence (@382 nm) of CzPy in the crystalline state at different temperature.

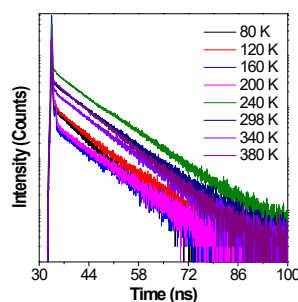


Figure S24. Time-resolved decay of the fluorescence (@400 nm) of CzPM in the crystalline state at different temperature.

Table S2. Fluorescence lifetime data of CzPh at 430 nm in the crystalline state under different temperature ($\lambda_{\text{ex}} = 320$ nm).

	298 K	240 K	200 K	160 K	120 K	80 K
τ_1 (ns)	14.4	14.3	14.9	14.8	16.2	15.7
τ_2 (ns)	87.6	100.0	104.0	103.5	108.9	106.9
τ (ns) ^a	50.5	55.7	59.4	61.5	67.0	65.6

^a τ = average fluorescence lifetime at 430 nm calculated by $\tau = \sum A_i \tau_i^2 / \sum A_i \tau_i$, where A_i is the pre-exponential factor for lifetime τ_i .

Table S3. Fluorescence lifetime data of CzPy at 382 nm in the crystalline state under different temperature ($\lambda_{\text{ex}} = 320$ nm).

	298 K	240 K	200 K	160 K	120 K	80 K
τ_1 (ns)	2.49	2.57	2.91	2.87	2.99	2.92
τ_2 (ns)	5.42	5.16	6.58	6.40	7.09	6.09
τ (ns) ^a	4.32	3.96	3.98	4.20	4.39	4.59

^a τ = average fluorescence lifetime at 430 nm calculated by $\tau = \sum A_i \tau_i^2 / \sum A_i \tau_i$, where A_i is the pre-exponential factor for lifetime τ_i .

Table S4. Fluorescence lifetime data of CzPM at 400 nm in the crystalline state under different temperature ($\lambda_{\text{ex}} = 350$ nm).

	380 K	340 K	298 K	240 K	200 K	160 K	120 K	80 K
τ (ns)	7.8	8.6	8.6	9.0	9.0	9.1	8.3	7.0

Table S5. Phosphorescence lifetime data of CzPh at 510 nm in the crystalline state under different temperature ($\lambda_{\text{ex}} = 320$ nm).

	298 K	240 K	200 K	160 K	120 K	80 K
τ_1 (ms)	/	/	450	1290	1307	1475
τ_2 (ms)	/	/	88	296	299	325
τ (ms) ^a	/	/	382	735	801	889

^a τ = average phosphorescence lifetime at 510 nm calculated by $\tau = \sum A_i \tau_i^2 / \sum A_i \tau_i$, where A_i is the pre-exponential factor for lifetime τ_i .

Table S6. Phosphorescence lifetime data of CzPh at 550 nm in the crystalline state under different temperature ($\lambda_{\text{ex}} = 320$ nm).

	298 K	240 K	200 K	160 K	120 K	80 K
τ_1 (ms)	150	1022	1014	1175	1325	1374
τ_2 (ms)	650	156	112	280	307	316
τ (ms) ^a	579	942	889	824	959	966

^a τ = average phosphorescence lifetime at 550 nm calculated by $\tau = \sum A_i \tau_i^2 / \sum A_i \tau_i$, where A_i is the pre-exponential factor for lifetime τ_i .

Table S7. Phosphorescence lifetime data of CzPh at 600 nm in the crystalline state under different temperature ($\lambda_{\text{ex}} = 320$ nm).

	298 K	240 K	200 K	160 K	120 K	80 K
τ_1 (ms)	660	126	117	1110	1248	267
τ_2 (ms)	119	1020	1015	245	278	1241
τ (ms) ^a	575	920	898	877	978	949

^a τ = average phosphorescence lifetime at 600 nm calculated by $\tau = \sum A_i \tau_i^2 / \sum A_i \tau_i$, where A_i is the pre-exponential factor for lifetime τ_i .

Table S8. Phosphorescence lifetime data of CzPy at 488 nm in the crystalline state under different temperature ($\lambda_{\text{ex}} = 320$ nm).

	298 K	240 K	200 K	160 K	120 K	80 K
τ_1 (ms)	21	135	88	237	255	252
τ_2 (ms)	63	822	1080	1340	1460	1424
τ (ms) ^a	52	662	330	411	591	647

^a τ = average phosphorescence lifetime at 488 nm calculated by $\tau = \sum A_i \tau_i^2 / \sum A_i \tau_i$, where A_i is the pre-exponential factor for lifetime τ_i .

Table S9. Phosphorescence lifetime data of CzPy at 550 nm in the crystalline state under different temperature ($\lambda_{\text{ex}} = 320$ nm).

	298 K	240 K	200 K	160 K	120 K	80 K
τ_1 (ms)	90	168	108	227	248	233
τ_2 (ms)	488	1060	1190	1268	1341	1314
τ (ms) ^a	197	985	946	710	806	808

^a τ = average phosphorescence lifetime at 550 nm calculated by $\tau = \sum A_i \tau_i^2 / \sum A_i \tau_i$, where A_i is the pre-exponential factor for lifetime τ_i .

Table S10. Phosphorescence lifetime data of CzPM at 400 nm in the crystalline state under different temperature ($\lambda_{\text{ex}} = 350$ nm).

	380 K	340 K	298 K	240 K	200 K	160 K	120 K	80 K
τ_1 (ms)	8	65	58	/	/	/	/	/
τ_2 (ms)	20	140	470	/	/	/	/	/
τ (ms) ^a	17	140	435	/	/	/	/	/

^a τ = average phosphorescence lifetime at 400 nm calculated by $\tau = \sum A_i \tau_i^2 / \sum A_i \tau_i$, where A_i is the pre-exponential factor for lifetime τ_i .

Table S11. Phosphorescence lifetime data of CzPM at 463 nm in the crystalline state under different temperature ($\lambda_{\text{ex}} = 350$ nm).

	380 K	340 K	298 K	240 K	200 K	160 K	120 K	80 K
τ_1 (ms)	/	/	71	717	532	72	392	119
τ_2 (ms)	/	/	773	71	74	423	72	344
τ (ms) ^a	/	/	713	583	426	323	187	330

^a τ = average phosphorescence lifetime at 463 nm calculated by $\tau = \sum A_i \tau_i^2 / \sum A_i \tau_i$, where A_i is the pre-exponential factor for lifetime τ_i .

Table S12. Phosphorescence lifetime data of CzPM at 530 nm in the crystalline state under different temperature ($\lambda_{\text{ex}} = 350$ nm).

	380 K	340 K	298 K	240 K	200 K	160 K	120 K	80 K
τ_1 (ms)	16	441	1311	1719	1860	170	144	333
τ_2 (ms)	53	151	/	/	/	1918	1979	1994
τ (ms) ^a	51	417	1311	1719	1860	1890	1918	1883

^a τ = average phosphorescence lifetime at 530 nm calculated by $\tau = \Sigma A_i \tau_i^2 / \Sigma A_i \tau_i$, where A_i is the pre-exponential factor for lifetime τ_i .

Table S13. Phosphorescence lifetime data of CzPh in the crystalline state under different environmental conditions ($\lambda_{\text{ex}} = 320$ nm).

	Vacuum		Air	
	550 nm	600 nm	550 nm	600 nm
τ_1 (ms)	105	88	150	660
τ_2 (ms)	833	777	650	119
τ (ms) ^a	749	642	579	575

^a τ = average phosphorescence lifetime calculated by $\tau = \Sigma A_i \tau_i^2 / \Sigma A_i \tau_i$, where A_i is the pre-exponential factor for lifetime τ_i .

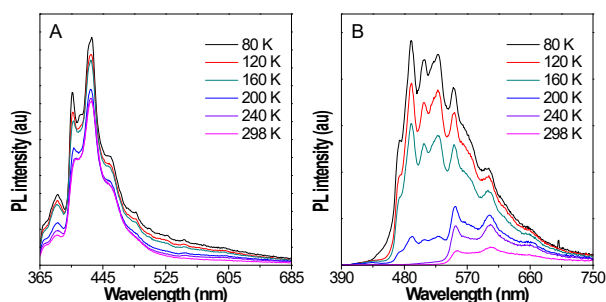
Table S14. Phosphorescence lifetime data of CzPy in the crystalline state under different environmental conditions ($\lambda_{\text{ex}} = 320$ nm).

	Vacuum		Air	
	550 nm	488 nm	550 nm	488 nm
τ_1 (ms)	109	59	90	21
τ_2 (ms)	849	186	488	63
τ (ms) ^a	721	147	197	52

^a τ = average phosphorescence lifetime calculated by $\tau = \Sigma A_i \tau_i^2 / \Sigma A_i \tau_i$, where A_i is the pre-exponential factor for lifetime τ_i .

Table S15. Phosphorescence lifetime data of CzPM in the crystalline state under different environmental conditions ($\lambda_{\text{ex}} = 350$ nm).

	Vacuum	Air
	530 nm	530 nm
τ (ms)	1342	1311

**Figure S25.** Prompt (A) and delayed (B) PL spectra of CzPh in the crystalline state under different temperature. The delayed PL spectra were taken after a delay of 50 ms.

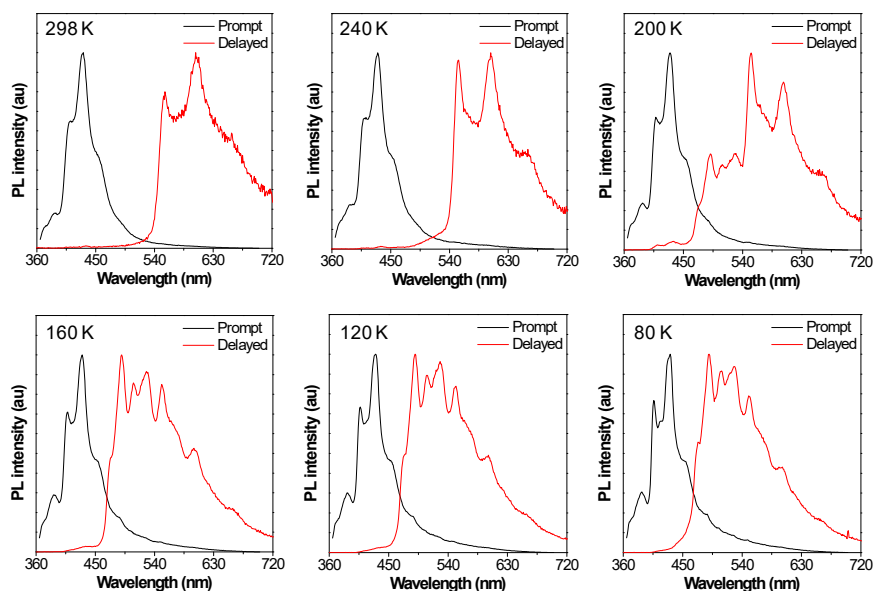


Figure S26. Normalized prompt and delayed PL spectra of CzPh in the crystalline state under different temperature. The delayed PL spectra were taken after a delay of 50 ms.

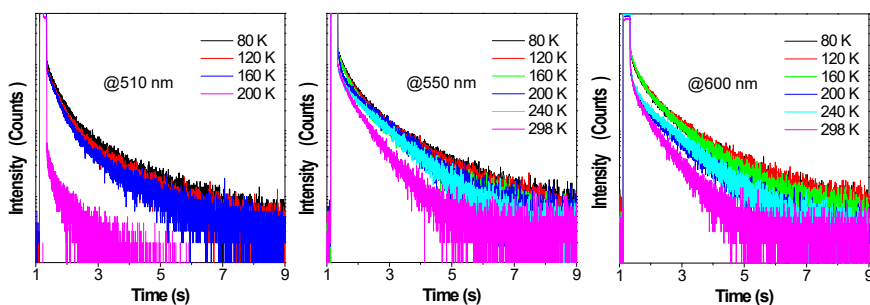


Figure S27. Time-resolved decay of the phosphorescence (@510nm, 550 nm and 600 nm) of CzPh in the crystalline state at different temperature.

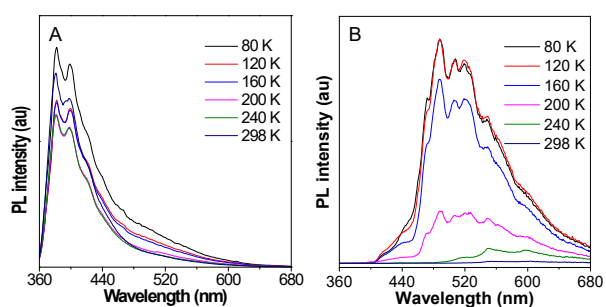


Figure S28. Prompt (A) and delayed (B) PL spectra of CzPy in the crystalline state under different temperature. The delayed PL spectra were taken after a delay of 50 ms.

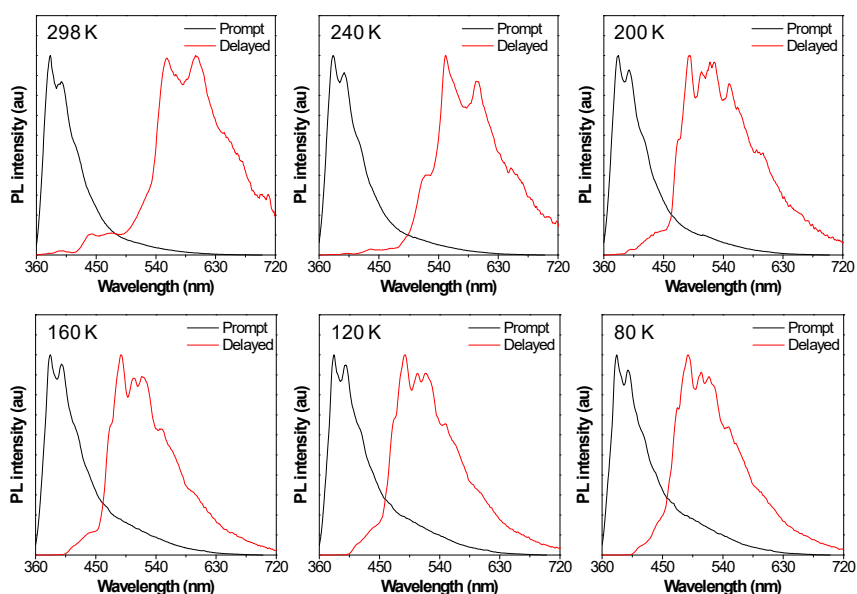


Figure S29. Normalized prompt and delayed PL spectra of CzPy in the crystalline state under different temperature. The delayed PL spectra were taken after a delay of 50 ms.

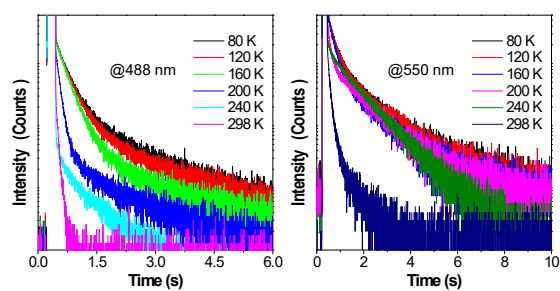


Figure S30. Time-resolved decay of phosphorescence (@488nm and 550 nm) of CzPy in the crystalline state at different temperature.

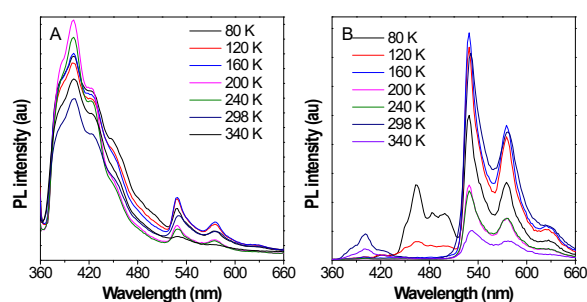


Figure S31. Prompt (A) and delayed (B) PL spectra of CzPM in the crystalline state under different temperature. The delayed PL spectra were taken after a delay of 50 ms.

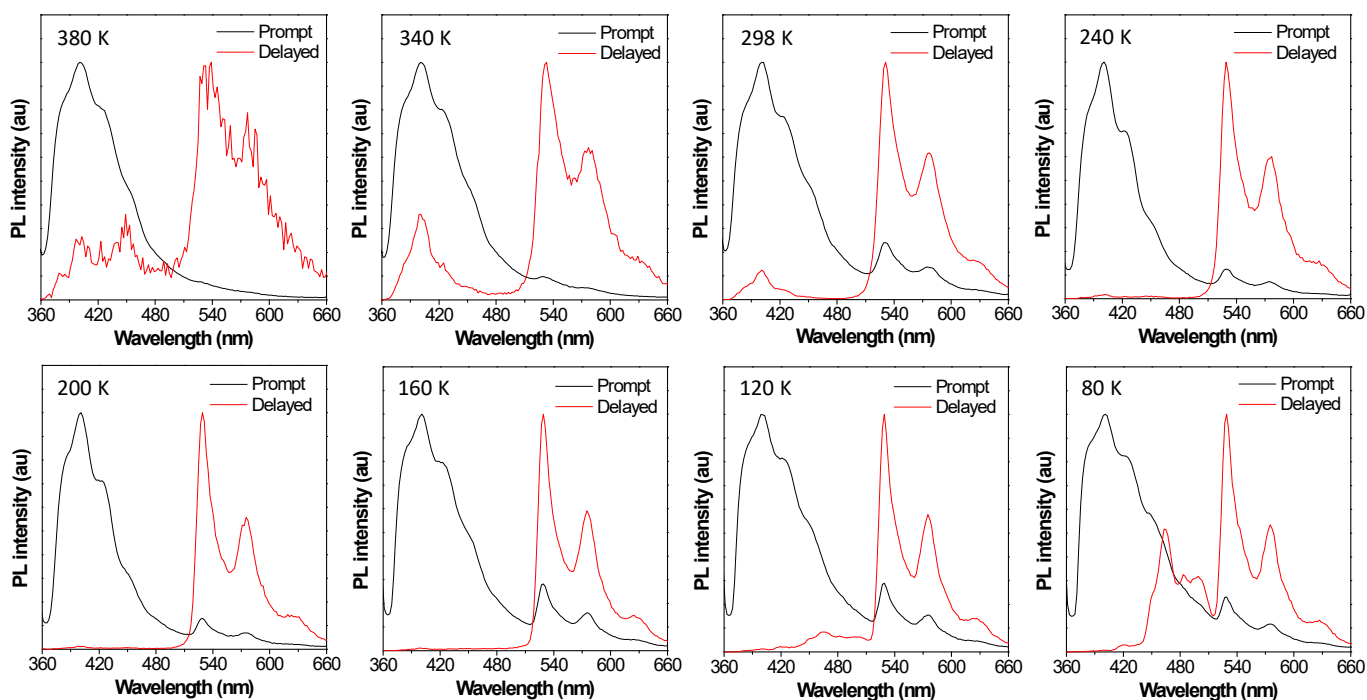


Figure S32. Normalized prompt and delayed PL spectra of CzPM in the crystalline state under different temperature. The delayed PL spectra were taken after a delay of 50 ms.

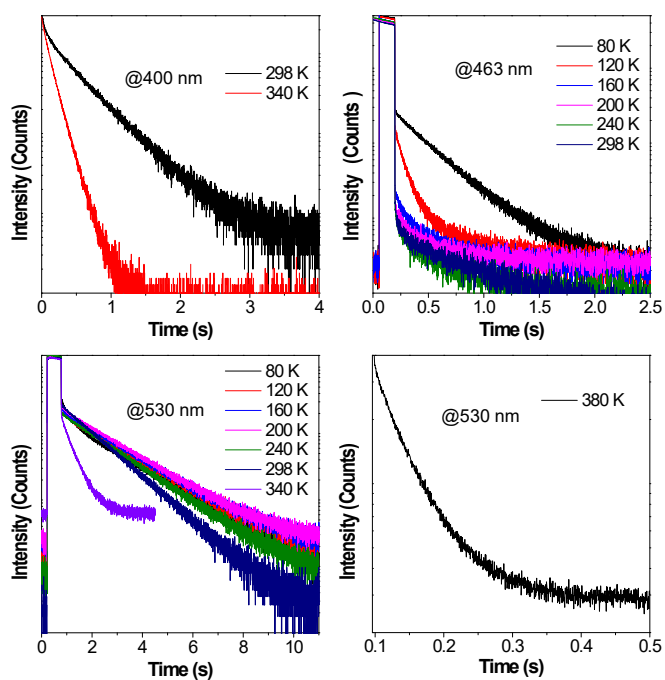


Figure S33. Time-resolved decay of the phosphorescence (@400, 463 nm and 530 nm) of CzPM in the crystalline state at different temperature.

Table S16. Fluorescence lifetime data of CzPhBr at 386 nm in the crystalline state under different temperature ($\lambda_{ex} = 320$ nm).

	298 K	240 K	200 K	160 K	120 K	80 K
τ_1 (ns)	1.33	1.41	1.48	1.48	1.62	1.60
τ_2 (ns)	3.73	3.72	5.12	3.46	5.10	4.49
τ (ns) ^a	1.49	1.62	1.68	1.74	1.87	2.01

^a τ = average fluorescence lifetime at 386 nm calculated by $\tau = \sum A_i \tau_i^2 / \sum A_i \tau_i$, where A_i is the pre-exponential factor for lifetime τ_i .

Table S17. Phosphorescence lifetime data of CzPhBr at 460 nm in the crystalline state under different temperature ($\lambda_{\text{ex}} = 320$ nm).

	298 K	240 K	200 K	160 K	120 K	80 K
τ_1 (ms)	38	43	29	90	111	246
τ_2 (ms)	191	239	220	478	716	76
τ_3 (ms)	/	/	/	/	/	959
τ (ms) ^a	150	143	96	303	489	431

^a τ = average phosphorescence lifetime at 460 nm calculated by $\tau = \sum A_i \tau_i^2 / \sum A_i \tau_i$, where A_i is the pre-exponential factor for lifetime τ_i .

Table S18. Phosphorescence lifetime data of CzPhBr at 550 nm in the crystalline state under different temperature ($\lambda_{\text{ex}} = 320$ nm).

	298 K	240 K	200 K	160 K	120 K	80 K
τ_1 (ms)	293	399	92	106	107	178
τ_2 (ms)	/	/	444	484	535	683
τ (ms) ^a	293	399	409	414	445	524

^a τ = average phosphorescence lifetime at 550 nm calculated by $\tau = \sum A_i \tau_i^2 / \sum A_i \tau_i$, where A_i is the pre-exponential factor for lifetime τ_i .

Table S19. Phosphorescence lifetime data of CzPhBr in the crystalline state under different environmental conditions ($\lambda_{\text{ex}} = 320$ nm).

	Vacuum		Air	
	550 nm	460 nm	550 nm	460 nm
τ_1 (ms)	326	47	293	38
τ_2 (ms)	/	383	/	191
τ (ms) ^a	326	213	293	150

^a τ = average phosphorescence lifetime calculated by $\tau = \sum A_i \tau_i^2 / \sum A_i \tau_i$, where A_i is the pre-exponential factor for lifetime τ_i .

Table S20. Fluorescence lifetime data of CzPyBr at 390 nm in the crystalline state under different temperature ($\lambda_{\text{ex}} = 320$ nm).

	298 K	240 K	200 K	160 K	120 K	80 K
τ_1 (ns)	5.33	4.86	4.10	4.91	0.72	3.95
τ_2 (ns)	53.61	63.24	64.26	64.99	4.29	66.08
τ_3 (ns)	0.65	0.66	0.66	0.72	69.77	0.71
τ (ns) ^a	20.25	28.20	31.72	20.78	39.59	24.09

^a τ = average fluorescence lifetime at 390 nm calculated by $\tau = \sum A_i \tau_i^2 / \sum A_i \tau_i$, where A_i is the pre-exponential factor for lifetime τ_i .

Table S21. Phosphorescence lifetime data of CzPyBr at 470 nm in the crystalline state under different temperature ($\lambda_{\text{ex}} = 320$ nm).

	298 K	240 K	200 K	160 K	120 K	80 K
τ_1 (ms)	60	35	83	107	128	133
τ_2 (ms)	/	123	258	346	461	437
τ (ms) ^a	60	113	176	176	217	308

^a τ = average phosphorescence lifetime at 470 nm calculated by $\tau = \sum A_i \tau_i^2 / \sum A_i \tau_i$, where A_i is the pre-exponential factor for lifetime τ_i .

Table S22. Phosphorescence lifetime data of CzPyBr at 510 nm in the crystalline state under different temperature ($\lambda_{\text{ex}} = 320$ nm).

	298 K	240 K	200 K	160 K	120 K	80 K
τ_1 (ms)	62	80	84	94	103	105
τ_2 (ms)	/	136	258	292	334	376
τ (ms) ^a	62	95	144	164	182	223

^a τ = average phosphorescence lifetime at 510 nm calculated by $\tau = \sum A_i \tau_i^2 / \sum A_i \tau_i$, where A_i is the pre-exponential factor for lifetime τ_i .

Table S23. Phosphorescence lifetime data of CzPyBr at 550 nm in the crystalline state under different temperature ($\lambda_{\text{ex}} = 320$ nm).

	298 K	240 K	200 K	160 K	120 K	80 K
τ_1 (ms)	65	81	86	92	98	98
τ_2 (ms)	/	138	259	288	319	349
τ (ms) ^a	65	95	137	154	174	197

^a τ = average phosphorescence lifetime at 550 nm calculated by $\tau = \sum A_i \tau_i^2 / \sum A_i \tau_i$, where A_i is the pre-exponential factor for lifetime τ_i .

Table S24. Phosphorescence lifetime data of CzPyBr in the crystalline state under different environmental conditions ($\lambda_{\text{ex}} = 320$ nm).

	Vacuum			Air		
	550 nm	510 nm	470 nm	550 nm	510 nm	470 nm
τ (ms)	72	68	67	65	62	60

Table S25. Fluorescence lifetime data of CzPMBr at 410 nm in the crystalline state under different temperature ($\lambda_{\text{ex}} = 350$ nm).

	298 K	240 K	200 K	160 K	120 K	80 K
τ_1 (ns)	0.39	0.62	0.58	0.66	1.06	0.71
τ_2 (ns)	3.59	4.02	4.06	4.34	5.69	4.78
τ (ns) ^a	3.26	3.78	3.44	3.54	4.18	3.27

^a τ = average fluorescence lifetime at 410 nm calculated by $\tau = \sum A_i \tau_i^2 / \sum A_i \tau_i$, where A_i is the pre-exponential factor for lifetime τ_i .

Table S26. Phosphorescence lifetime data of CzPMBr at 530 nm in the crystalline state under different temperature ($\lambda_{\text{ex}} = 350$ nm).

	298 K	240 K	200 K	160 K	120 K	80 K
τ_1 (ms)	150	166	166	163	155	138
τ_2 (ms)	417	582	593	594	586	554
τ (ms) ^a	233	278	305	322	344	335

^a τ = average phosphorescence lifetime at 530 nm calculated by $\tau = \sum A_i \tau_i^2 / \sum A_i \tau_i$, where A_i is the pre-exponential factor for lifetime τ_i .

Table S27. Phosphorescence lifetime data of CzPMBr in the crystalline state under different environmental conditions ($\lambda_{\text{ex}} = 350 \text{ nm}$).

	Vacuum	Air
	530 nm	530 nm
τ_1 (ms)	154	150
τ_2 (ms)	425	417
τ_a (ms)	235	233

^a $\tau =$ average phosphorescence lifetime calculated by $\tau = \Sigma A_i \tau_i^2 / \Sigma A_i \tau_i$, where A_i is the pre-exponential factor for lifetime τ_i .

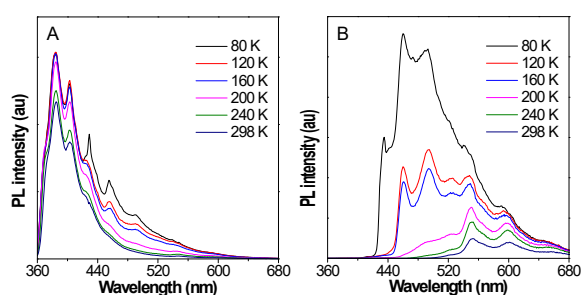


Figure S34. Prompt (A) and delayed (B) PL spectra of CzPhBr in the crystalline state under different temperature. The delayed PL spectra were taken after a delay of 50 ms.

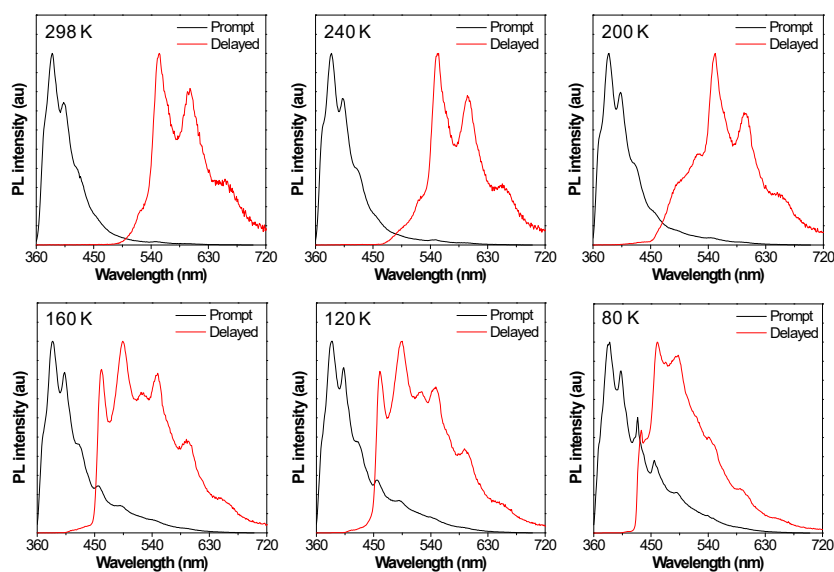


Figure S35. Normalized prompt and delayed PL spectra of CzPhBr in the crystalline state under different temperature. The delayed PL spectra were taken after a delay of 50 ms.

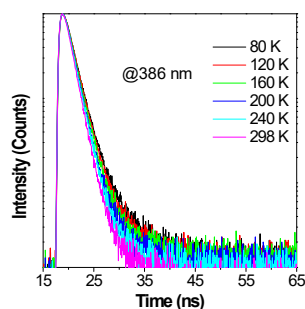


Figure S36. Time-resolved decay of the fluorescence (@386 nm) of CzPhBr in the crystalline state at different temperature.

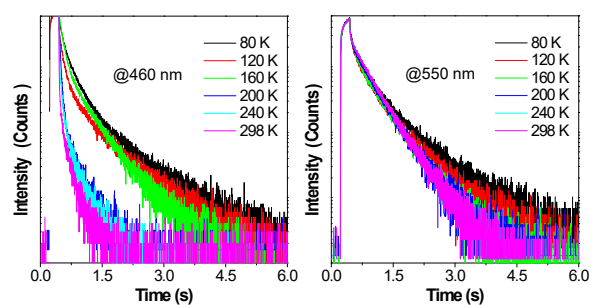


Figure S37. Time-resolved decay of the phosphorescence (@460 nm and 550 nm) of CzPhBr in the crystalline state at different temperature.

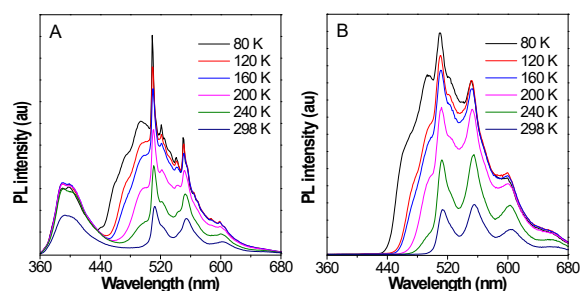


Figure S38. Prompt (A) and delayed (B) PL spectra of CzPyBr in the crystalline state under different temperature. The delayed PL spectra were taken after a delay of 50 ms.

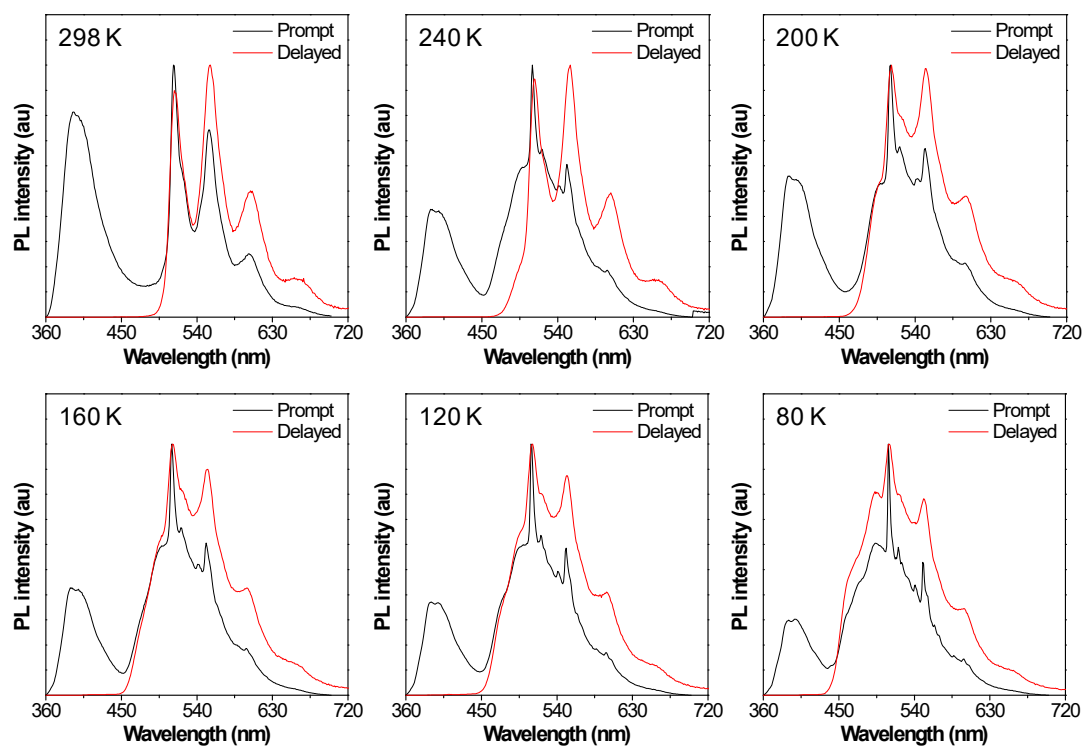


Figure S39. Normalized prompt and delayed PL spectra of CzPyBr in the crystalline state under different temperature. The delayed PL spectra were taken after a delay of 50 ms.

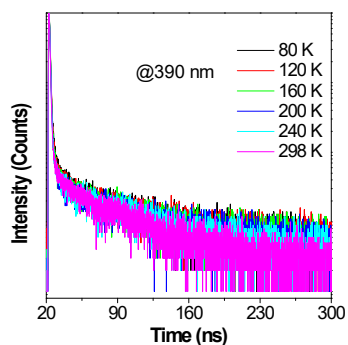


Figure S40. Time-resolved decay of the fluorescence (@390 nm) of CzPyBr in the crystalline state at different temperature.

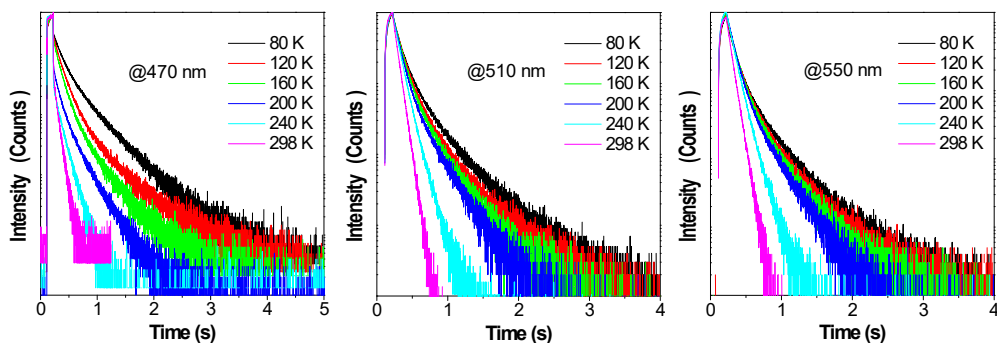


Figure S41. Time-resolved decay of the phosphorescence (@470 nm, 510 nm and 550 nm) of CzPyBr in the crystalline state at different temperature.

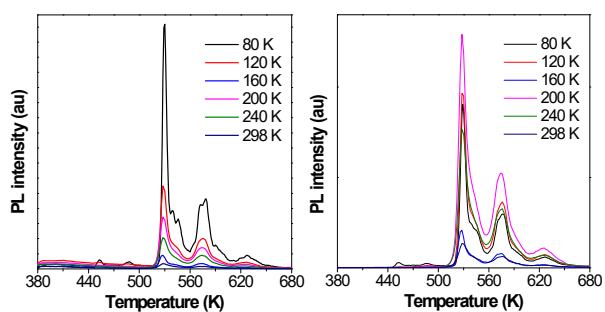


Figure S42. Prompt (A) and delayed (B) PL spectra of CzPMBr in the crystalline state under different temperature. The delayed PL spectra were taken after a delay of 50 ms.

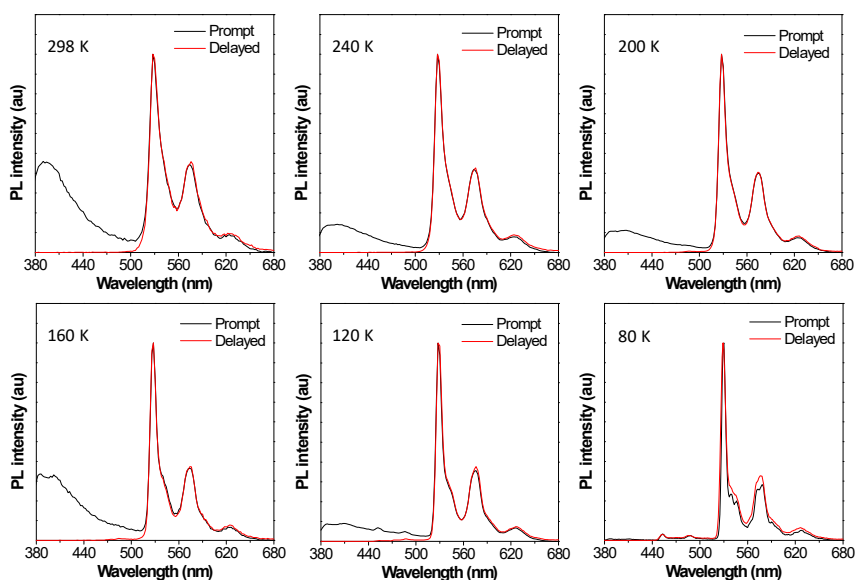


Figure S43. Normalized prompt and delayed PL spectra of CzPMBr in the crystalline state under different temperature. The delayed PL spectra were taken after a delay of 50 ms.

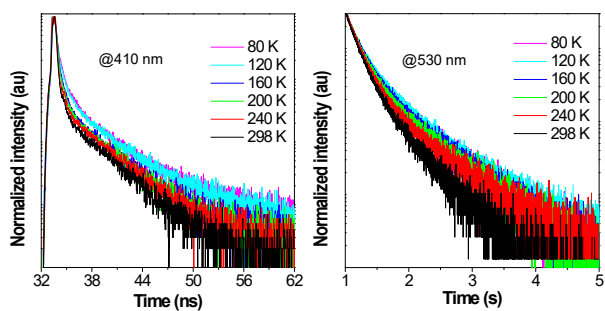


Figure S44. Time-resolved decay of the fluorescence (@410 nm) and phosphorescence (@530 nm) of CzPMBr in the crystalline state at different temperature.

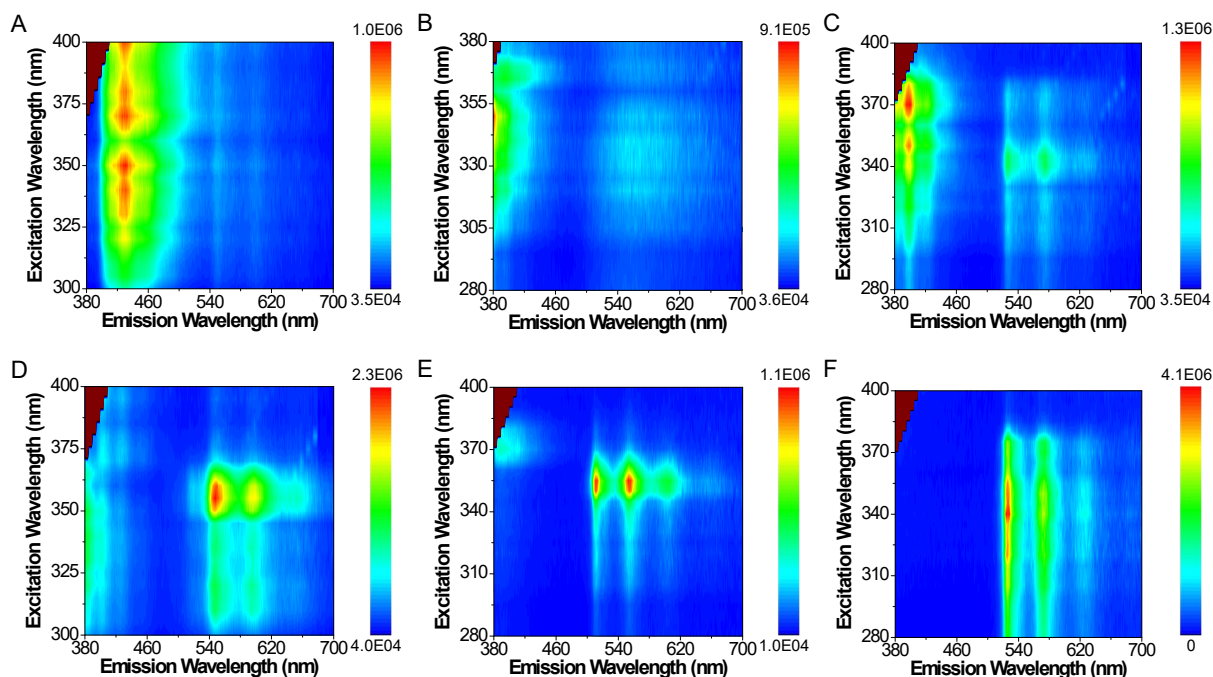


Figure S45. Phosphorescence spectra of CzPh (A), CzPy (B), CzPM (C), CzPhBr (D), CzPyBr (E) and CzPMBr (F) in the crystalline state upon different excitation wavelength.

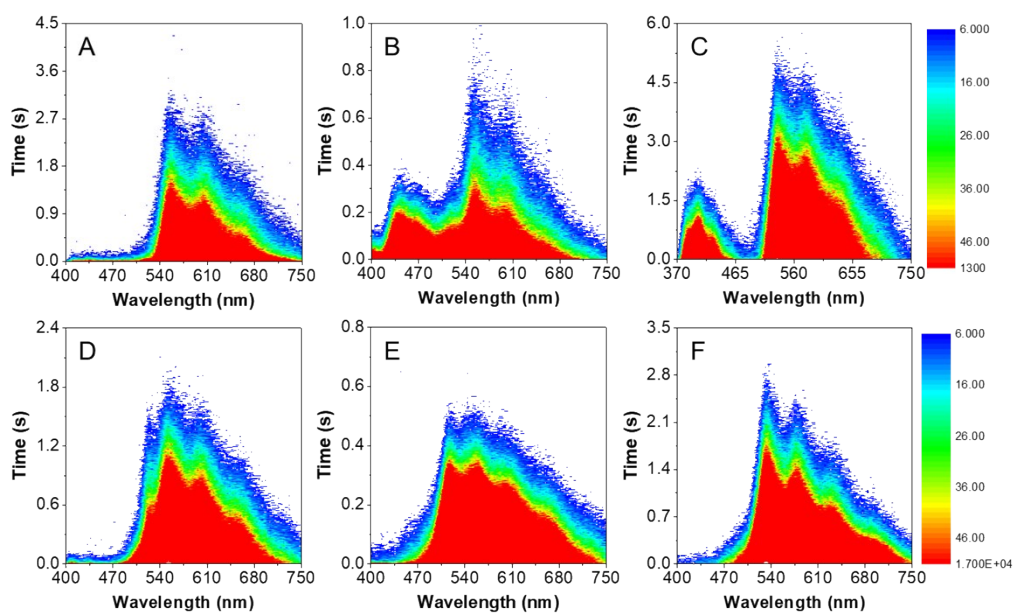


Figure S46. Time-resolved emission spectra of CzPh (A), CzPy (B), CzPM (C), CzPhBr (D), CzPyBr (E) and CzPMBr (F) in the crystalline state excited at room temperature.

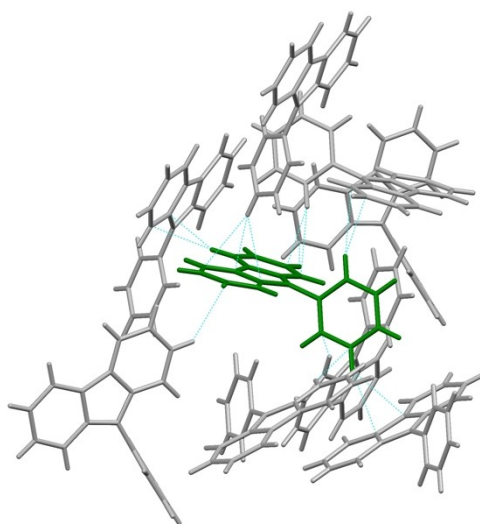


Figure S47. C-H... π interactions and other short contacts in the single crystal of CzPh.

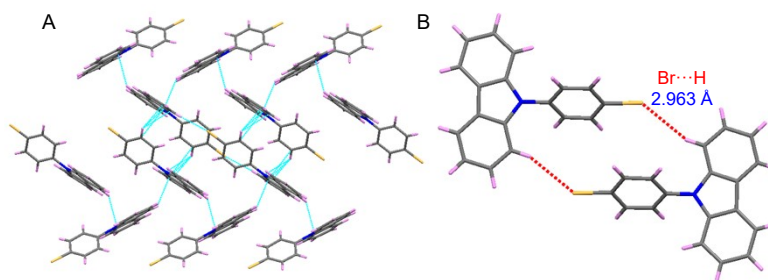


Figure S48. (A) Intermolecular packing, short contacts and (B) Br-H interactions in the single crystal of CzPhBr.

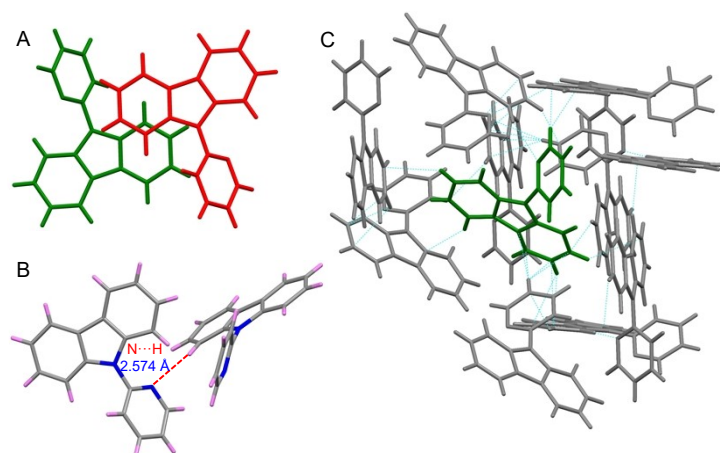


Figure S49. (A) π - π , (B) $N\cdots H$, (C) $C-H\cdots\pi$ interactions and other short contacts in the single crystal of CzPy.

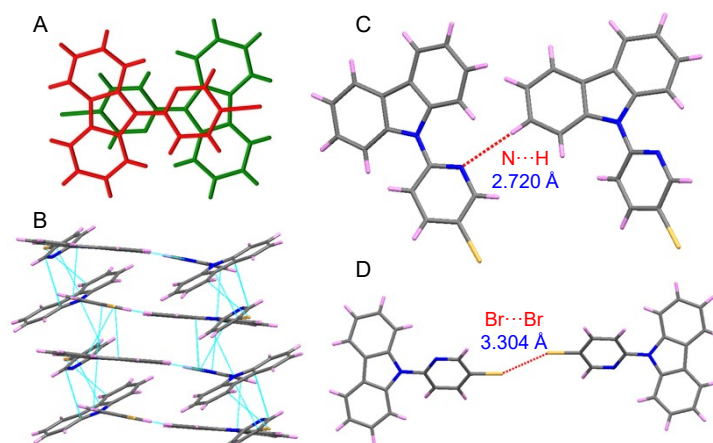


Figure S50. (A) π - π interactions, (B) intermolecular packing, other short contacts, (C) $N\cdots H$ interactions, and (D) $C-H\cdots\pi$ interactions in the single crystal of CzPyBr.

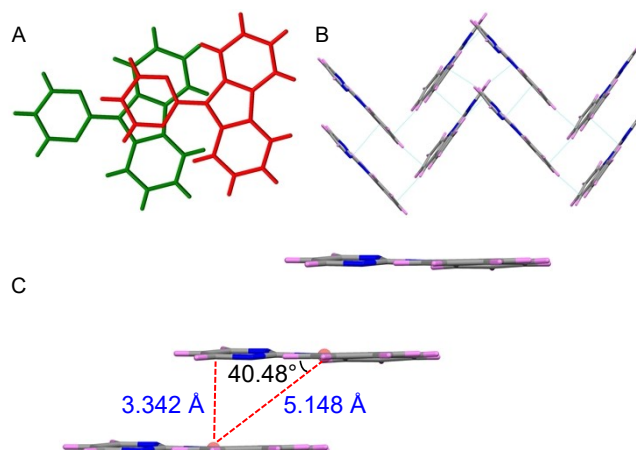


Figure S51. (A) π - π interactions, (B) intermolecular packing, other short contacts and (C) J-aggregates in the single crystal of CzPM.

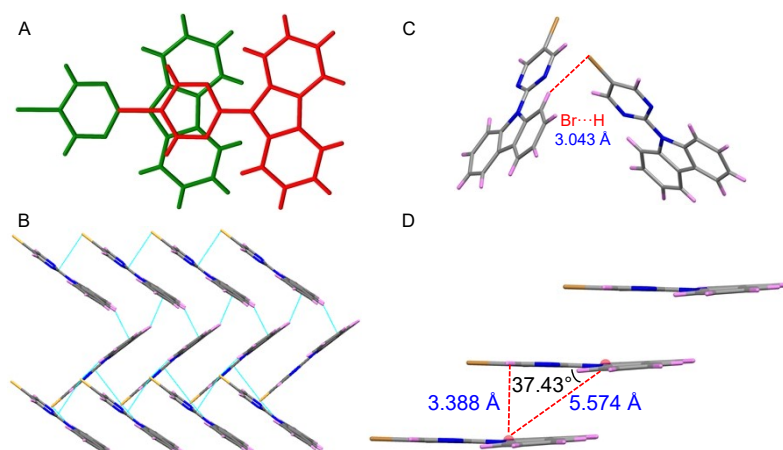


Figure S52. (A) π - π interactions, (B) intermolecular packing, other short contacts, (C) Br \cdots H interactions and (D) J-aggregates in the single crystal of CzPMBr.

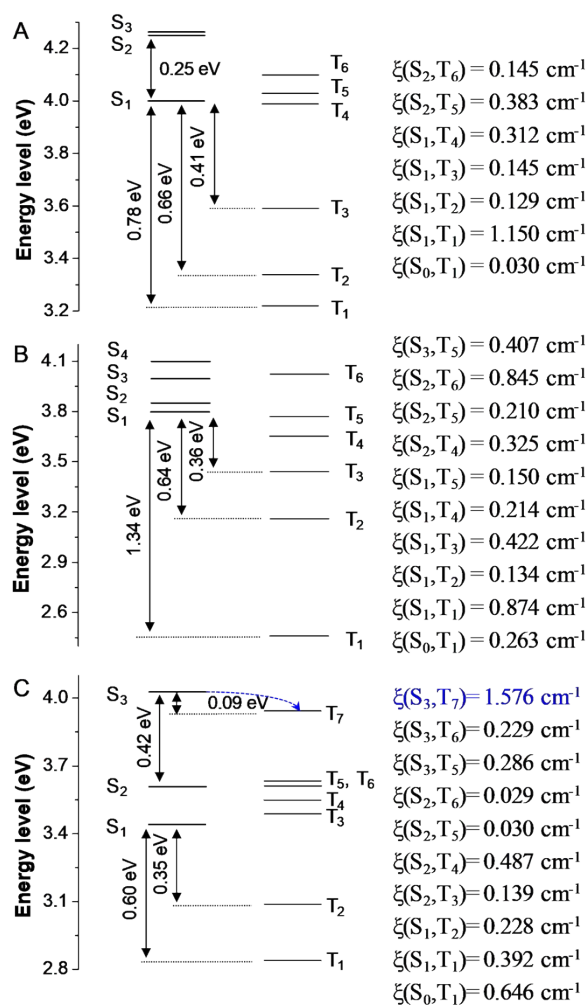


Figure S53. Schematic diagrams of the TD-DFT calculated energy levels, possible HISC channels and spin-orbit coupling matrix elements (ξ) of CzPh (A), CzPy (B) and CzPM (C).

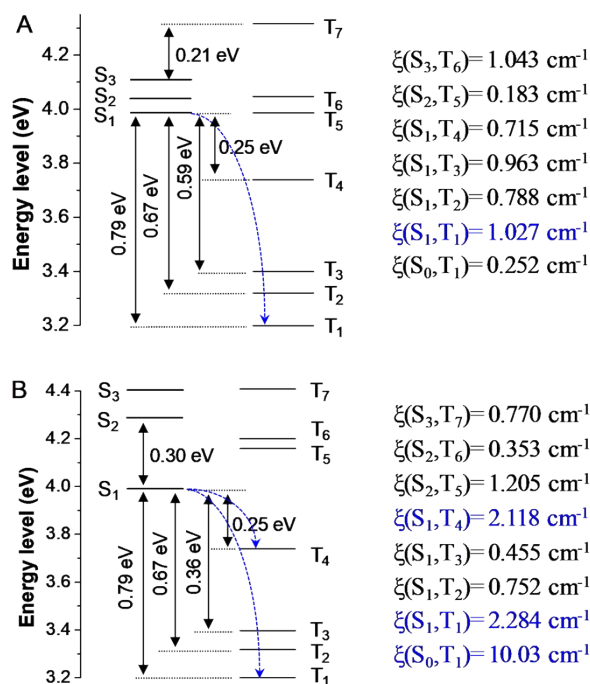


Figure S54. Schematic diagrams of the TD-DFT calculated energy levels, possible HISC/ISC channels and spin-orbit coupling matrix elements (ξ) of CzPhBr (A) and CzPyBr (B).

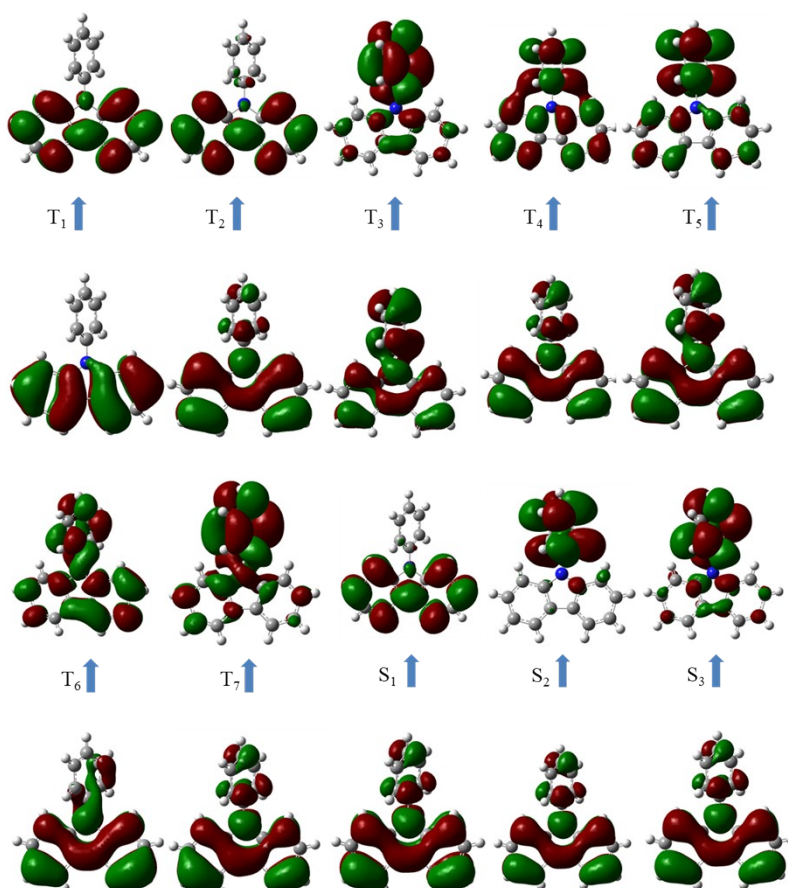


Figure S55. The NTOs of CzPh at the optimized T₁ geometric structures.

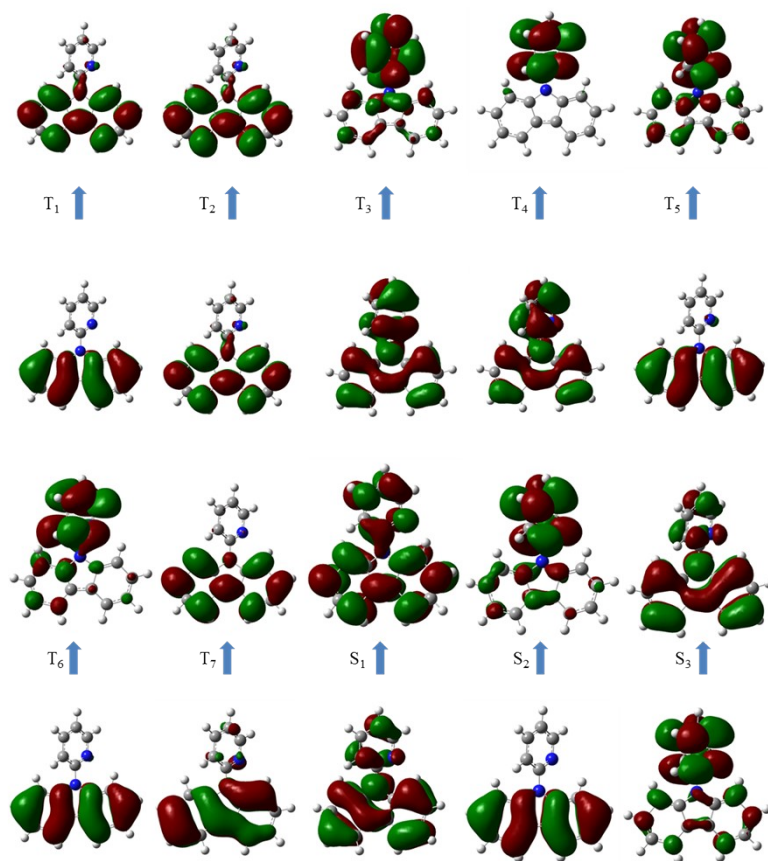


Figure S56. The NTOs of CzPy at the optimized T_1 geometric structures.

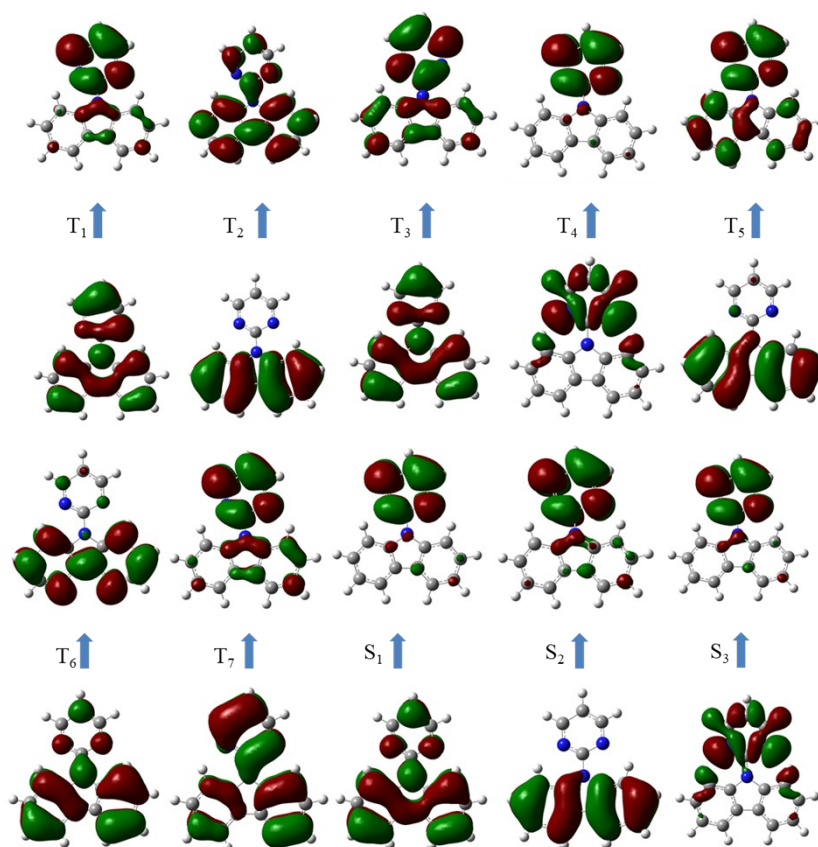


Figure S57. The NTOs of CzPM at the optimized T_1 geometric structures.

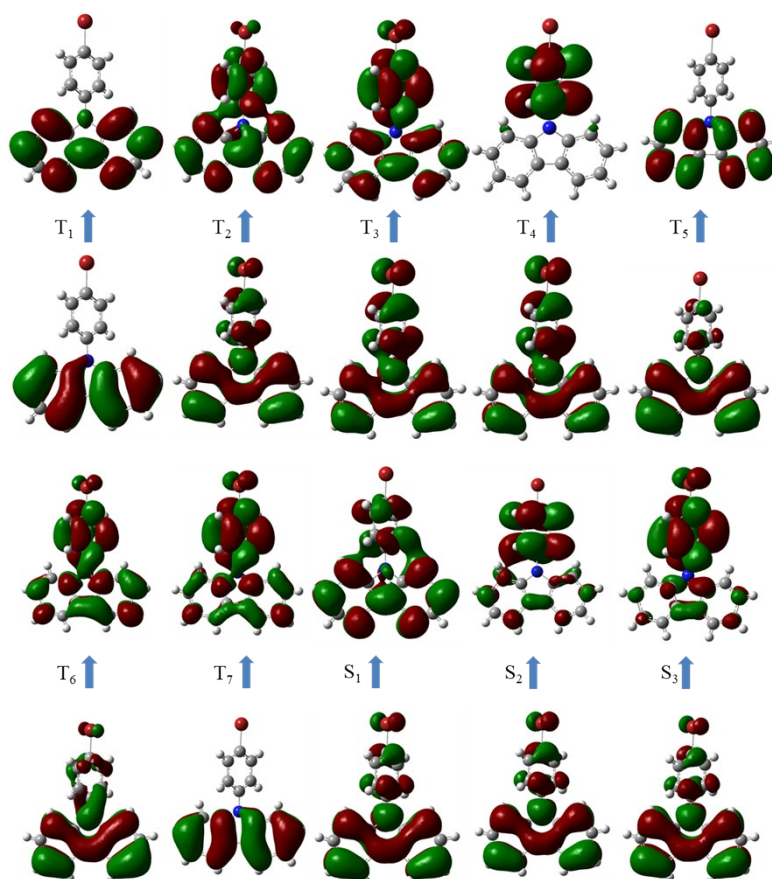


Figure S58. The NTOs of CzPhBr at the optimized T_1 geometric structures.

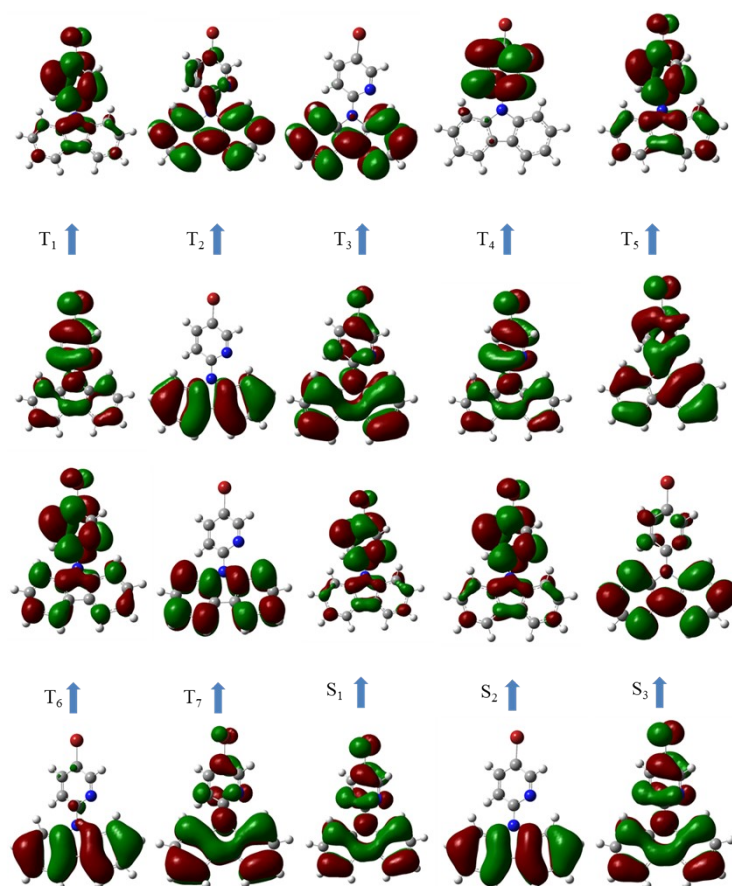


Figure S59. The NTOs of CzPyBr at the optimized T_1 geometric structures.

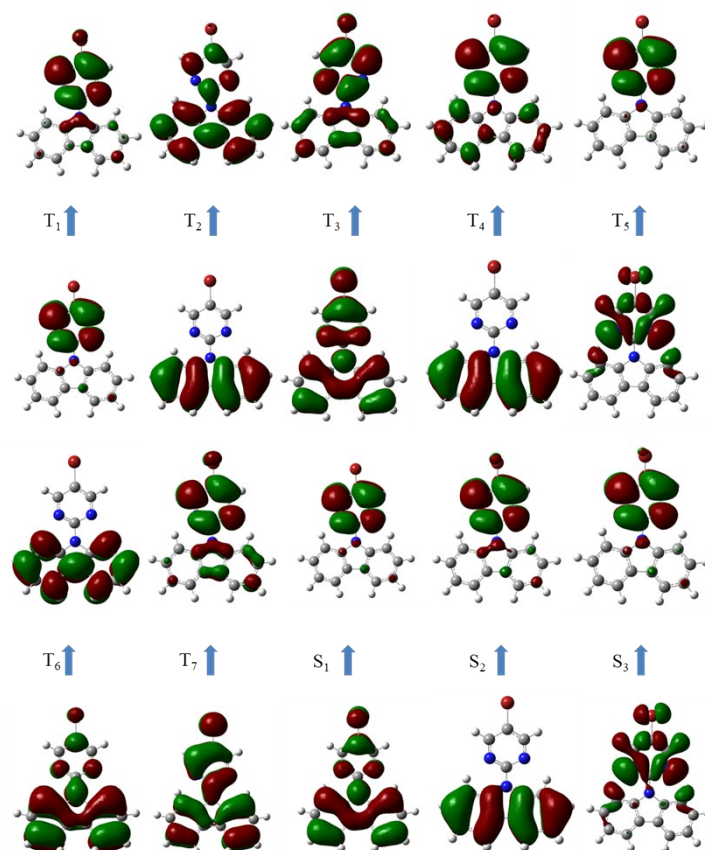


Figure S60. The NTOs of CzPMBr at the optimized T_1 geometric structures.

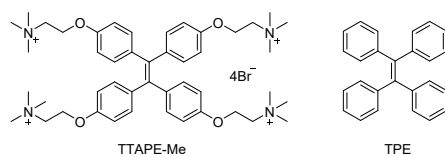


Figure S61. The chemical structures of TTAPE-Me and TPE.

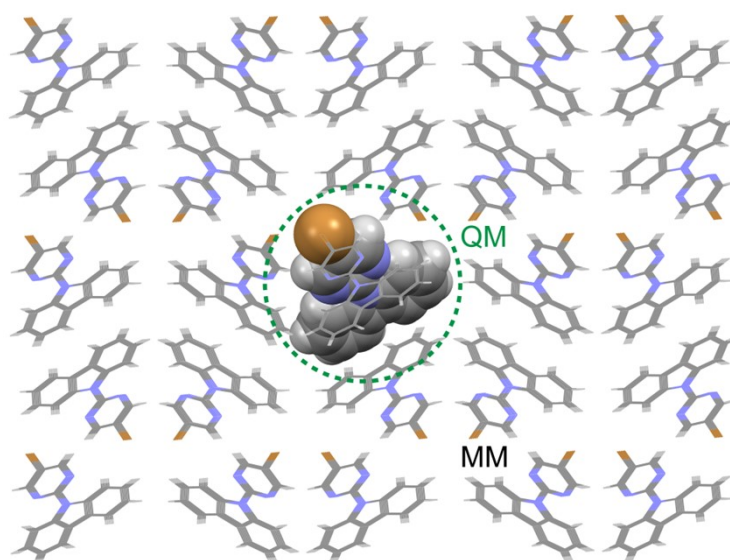


Figure S62. Setup of QM/MM model (taking CzPMBr as an example)

- [1] Liu W, Wang F, Li L. *J Theor Comput Chem* 2003; 2:257–72.
- [2] Liu W, Hong G, Dai D, Li L, Dolg M. *Theor Chem Accounts* 1997; 96:75–83.
- [3] Frisch MJ, Trucks GW, Schlegel HB, Scuseria GE, Robb MA, Cheeseman JR, et al. *Gaussian 09 revision C.01*. Wallingford, CT: Gaussian, Inc.; 2009.